RECEPTIVITY STUDIES ON A SWEPT-WING MODEL

A Thesis

by

MATTHEW JEFFERY WOODRUFF

Submitted to the Office of Graduate Studies of
Texas A&M University
in partial fulfillment of the requirements for the degree of

MASTER OF SCIENCE

May 2011

Major Subject: Aerospace Engineering

RECEPTIVITY STUDIES ON A SWEPT-WING MODEL

A Thesis

by

MATTHEW JEFFERY WOODRUFF

Submitted to the Office of Graduate Studies of
Texas A&M University
in partial fulfillment of the requirements for the degree of

MASTER OF SCIENCE

Approved by:

Chair of Committee,   William Saric
Committee Members,   Edward White
    Andrew Duggleby
Head of Department,   Dimitris Lagoudas

May 2011

Major Subject: Aerospace Engineering

ABSTRACT

Receptivity Studies on a Swept-Wing Model. (May 2011)

Matthew Jeffery Woodruff, B.S., Milwaukee School of Engineering

Chair of Advisory Committee: Dr. William Saric

A series of flight tests was performed using a swept-wing model mounted on a Cessna O-2 aircraft. The crossflow waves on the airfoil were excited by pneumatic spanwise-periodic distributed roughness elements (DREs). The objective of the experiment was to determine the roughness receptivity i.e. the relationship between roughness height and the amplitude of the unstable crossflow wave. The local skin-friction variation was measured using an array of calibrated and temperature-compensated hotfilm sensors. The amplitudes of the disturbance shear stress were compared to the amplitudes of the DREs. It was found that there is a relationship between the shear stress and DRE amplitude that needs to be studied more before any definitely conclusions can be made. It was also found that the sensitivity of the crossflow to DREs is highly dependent on the freestream turbulence levels.

ACKNOWLEDGEMENTS

First of all, I would like to thank Dr. William Saric, who provided me with the opportunity to do this research, and guided me along the way. His guidance and demand for perfection taught me so much, and helped me to become a better engineer.

Thank you also to my two committee members, Dr. Ed White and Dr. Andrew Duggleby, for providing support throughout my time at Texas A&M. Thank you also to Dr. Helen Reed, for providing computations and guidance in the analysis of the results of the experiments.

I would like to acknowledge the support of the student workers who helped out in supporting flight operations throughout my time at the Flight Research Lab. Thanks to the many early mornings, we were able to accomplish so much. Thank you especially to Andrew Carpenter, who guided and taught me in my first few months, and taught me the value of hard work and dedication. Thank you to Rob Downs for his help with the spectral analysis of the data. I would also like to acknowledge the future FRL students, Josh Fanning, Simon Hedderman, and Tom Williams, who will be continuing the work of the FRL. Best of luck to them.

Finally, thank you so much to our support staff, including our mechanic Cecil Rhodes, and our administrative assistants Colleen Leatherman and Kelli Perry. Cecil provided

knowledge and guidance, taught me the ways of an A&P mechanic, and most importantly kept the O-2 flying. Without Colleen and Kelli, I'm sure the FRL and wind tunnels could not function properly, and I am eternally grateful for all the help with travel arrangements, purchasing, and general support.

NOMENCLATURE

Re_c chord Reynolds number

Λ leading edge sweep

α aircraft angle of attack

β aircraft sideslip angle

AoA   SWIFT model angle of attack

KIAS   knots indicated airspeed

KTAS   knots true airspeed

x/c   percent chord location

p   static pressure

q   dynamic pressure

C_p coefficient of pressure

DRE   discrete roughness element

PDRE   pneumatic discrete roughness element

TABLE OF CONTENTS

LIST OF FIGURES

Page

Page

CHAPTER I

INTRODUCTION AND PREVIOUS WORK

MOTIVATION

The crossflow instability is the last major hurdle in swept-wing laminar flow control
(SWLFC) (Saric & Reed 2003) in controlling the amplitude of disturbances that cause
transition to turbulence, and progress has been made recently in developing distributed
roughness element (DRE) technology (Carpenter *et al*. 2009) to delay the transition to
turbulence on swept wings. One large hurdle still standing is understanding the
receptivity step in the process of laminar to turbulent transition i.e. how micron-sized
surface roughness creates the initial amplitudes of unstable crossflow waves. When the
relationship is established between leading-edge roughness and crossflow waves,
nonlinear stability calculations can be validated for the prediction of amplitude growth.

Currently, linear stability theory is used to design natural laminar flow airfoils. While
both the linear Orr-Sommerfeld equation and linear parabolized stability equations
provide a good estimate to the disturbance amplitude, it has been shown (as seen in
Figure 1) that the non-linear parabolized stability equations (NPSE) provide a much
better estimate of the disturbance level as compared to experiments. However, in order
to use NPSE, it is required to know the coupling between leading edge roughness and

_____

This thesis follows the style of *Journal of Fluid Mechanics*.

the crossflow amplitude downstream. It is easy to do this in a wind tunnel with detailed

leading edge boundary layer scans, but in flight a different method must be used.
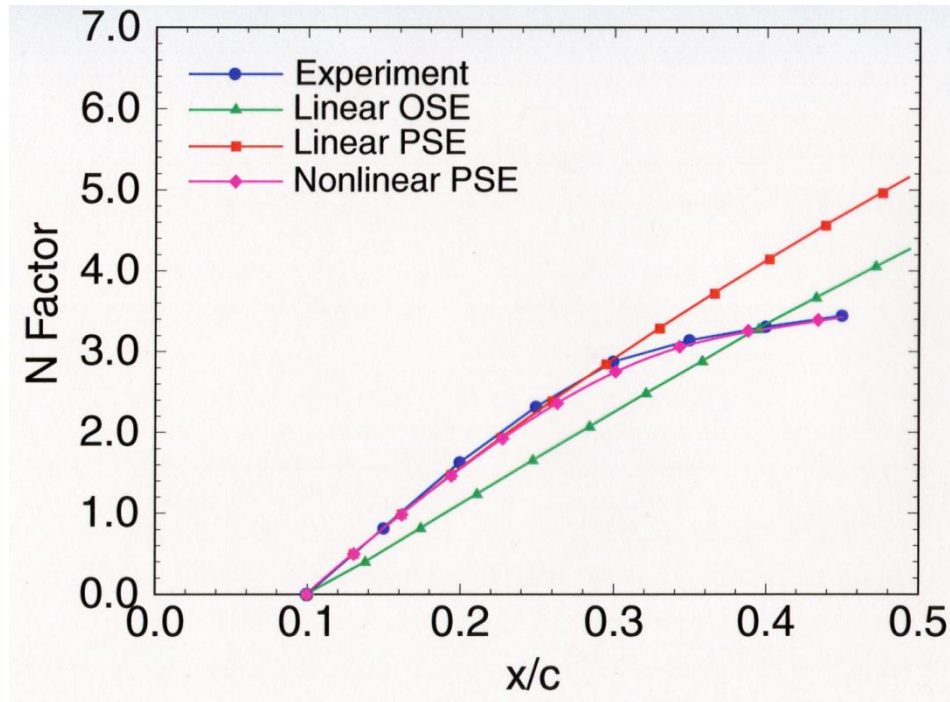
Figure 1: Linear and non-linear solvers compared to experimental results

It is well known that laminar flow over a wing produces less drag than a turbulent

boundary layer. With less drag comes reduced fuel consumption and higher efficiency,

bringing down operating costs for aircraft, especially long-haul cargo and passenger

aircraft. The tools for analyzing laminar to turbulent transition are not completely

accurate, as there are many different factors that affect the transition location. Knowing

more about one such factor (leading edge surface roughness), puts us one step closer to understanding the physics behind laminar to turbulent transition.

The ideal environment for experimenting with laminar to turbulent transition work is a low disturbance environment, and it has been found that flight disturbance levels are on the order of 0.05%, and are therefore ideal for this type of research. There are approximately 6 wind tunnels in the world that are low disturbance as well, but all are low Reynolds number.

LITERATURE REVIEW

As the airflow around an airfoil passes over the leading edge, the process by which disturbances enter the boundary layer is known as receptivity. Receptivity is the least understood step in the process to transition to turbulence, and also has many benefits from being understood. One aspect of receptivity that can be measured is the crossflow amplitude related to the roughness height on the leading edge.

Work has been performed to measure the crossflow spacing by analyzing the RMS voltage of hotfilm sensors, as in Mangalam *et al*. (1990) and Agarwal *et al*. (1992). However, the amplitude of the crossflow is not able to be compared between sensors, as the resistance of each sensor is different, and to accurately analyze the amplitude, the hotfilm must be calibrated.

Reibert *et al*. (1996) measured crossflow amplitudes in the ASU Unsteady Wind Tunnel, and found that saturation occurs independently of roughness height, which was backed up by the calculations of Haynes & Reed (2000). This work did not measure the amplitude of the crossflow in the unsaturated region of the airfoil, which is the main component of understanding receptivity.

Carpenter *et al*. (2009) laid the ground work necessary to conduct experiments to determine receptivity coefficients in the unsaturated crossflow region. Hotfilms were used to measure the shear stress variations from crossflow in the saturated region of a laminar flow airfoil, and a calibration scheme was created to determine the amplitude of the crossflow. This calibration scheme is used in this thesis to measure amplitude against roughness height.

PREVIOUS WORK

Carpenter *et al*. (2009) discusses the work previously done with the SWIFT model, including determining the test conditions in flight, going through the airfoil design, and completing preliminary receptivity measurements in the crossflow saturated region. This chapter discusses the work relevant to the current experiment.

The Swept-Wing In Flight Testing (SWIFT) model is an airfoil that has been designed to be subcritical to all instabilities except for crossflow, and due to the low-disturbance environment of flight, is an ideal test platform for receptivity measurements. A system

was developed to actively control DRE height along the leading edge, and measure the resultant crossflow vortices generated by the DREs.

TEST CONDITIONS

In order to determine the feasibility of a crossflow experiment and to determine the initial conditions for calculations, a series of flights were conducted to measure the freestream disturbance levels in flight. The crossflow disturbance is very sensitive to freestream turbulence, so before experiments could commence, the conditions of the atmosphere needed to be measured.

A hotwire mount was manufactured and mounted on the Cessna O-2 in the proposed location of the test airfoil on the port wing, as seen in Figure 2. This mount was a symmetric airfoil with four available supports for hotwires, along with an RTD for total temperature measurements. On the starboard wing, an air data boom was mounted to measure α, β, p and q, which could then be used to calculate *KTAS*.
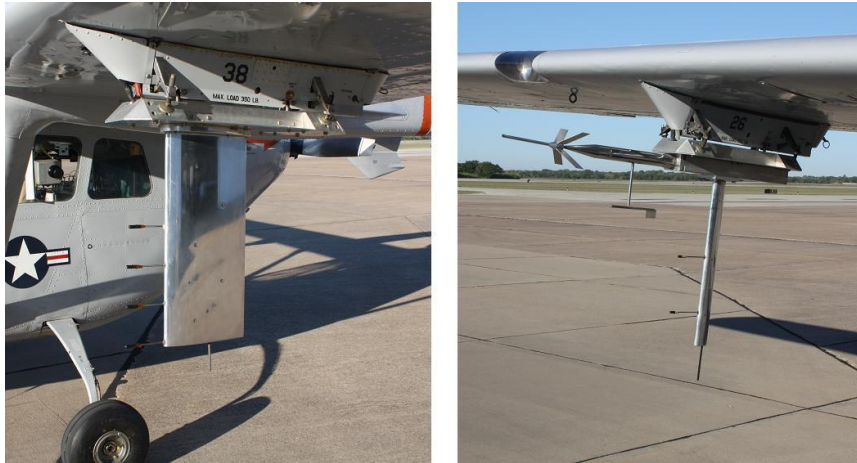
Figure 2: Hotwire sting mount on port wing and air data boom on starboard wing

Two hotwires were mounted to the sting mount and connected to a constant temperature anemometer and filter in the aircraft. A flight was performed to gather data at four different altitudes. In order to compensate for the different temperatures at the different altitudes, calibration data was recorded in the climb at each altitude, and the freestream measurement data was recorded in a high speed dive.

The freestream disturbance level was measured to be 0.05% to 0.07% of the freestream velocity between 158 and 168 *KTAS*. These values include turbulence and electronic noise, and were considered to be low enough to quantify the flight environment as low-disturbance.

C_p MEASUREMENTS

Along with the experimental work documented in Carpenter *et al*. (2009), extensive

CFD work was completed as documented in Rhodes *et al.* (2008). Before testing could

being, the flow over the test airfoil had to be verified with CFD, so detailed boundary

layer stability computations could be completed with the basic state of the airfoil. Also, a

proper *AoA* was needed that provided sufficient crossflow for the research to be done on

the airfoil. A pressure minimum at 70% with accelerated flow to that point was desired

for ideal testing conditions.

The Swept-Wing In Flight Testing (SWIFT) model is an airfoil that has been designed to

be subcritical to all instabilities except for crossflow, and due to the low-disturbance

environment of flight, is an ideal test platform for receptivity measurements. A system

was developed to actively control DRE height along the leading edge, and measure the

resultant crossflow vortices generated by the DREs.
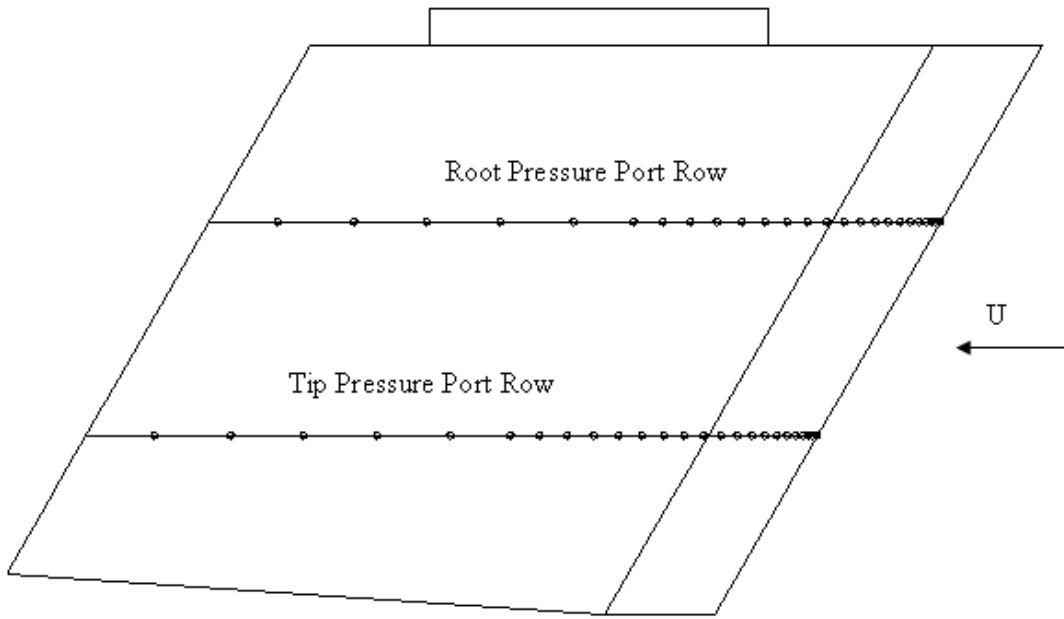
Note: Pressure Ports not Drawn to Scale

Figure 3: Pressure port locations on the SWIFT model

The SWIFT model has two rows of 32 pressure ports each, one located 13 inches from the root, and the other located 29 inches from the root as seen in Figure 3. This left a 16 inch region that was designated the area of focus for the research conducted on the model. The ports were of the highest density at the leading edge, and increased the spacing as the chord location increased.

C_p values were recorded at test points between AoA = -5° and AoA = 2°. Figures 4 and 5 show three different angles of attack – the two extreme cases and an intermediate case. The highest angle of attack tested was 2°. At this test point, the C_p distribution was starting to show a suction peak near the leading edge and a generally flat profile, both of which are not conducive to crossflow dominated flow. The lowest angle of attack shown is of great interest to the testing, as it has a strong accelerated pressure gradient back to the pressure minimum, and also showed strong crossflow growth in calculations. The intermediate angle of attack was shown to demonstrate the trend of the C_p distribution as the AoA was decreased.
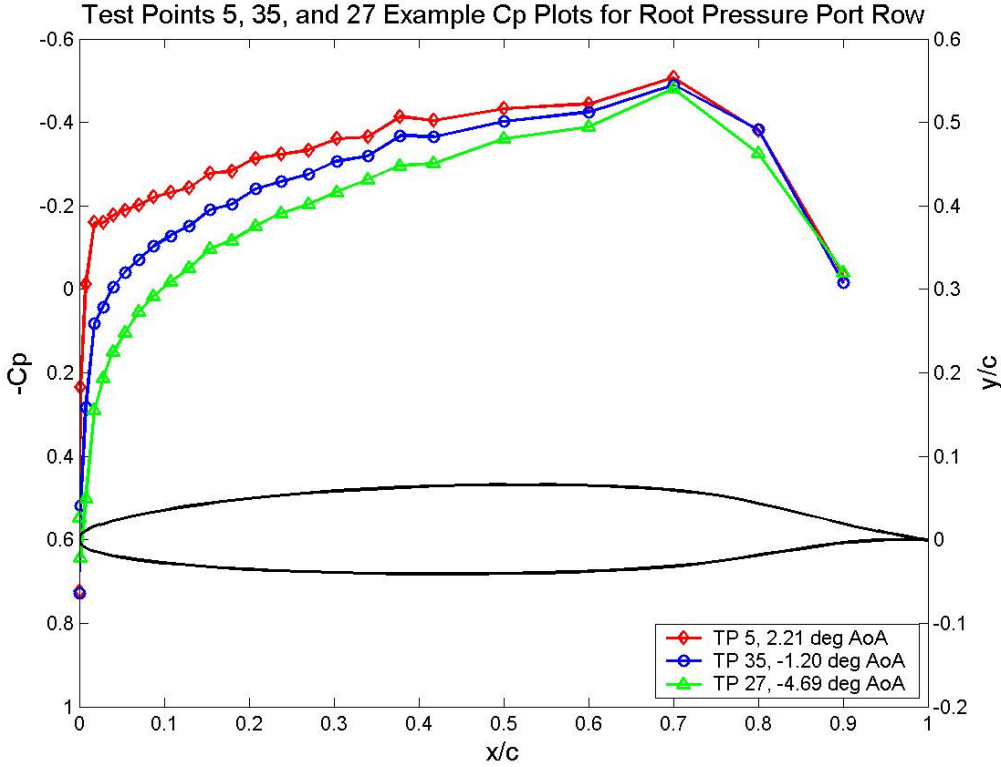
Figure 4: C_p data for root pressure row at three different *AoAs*
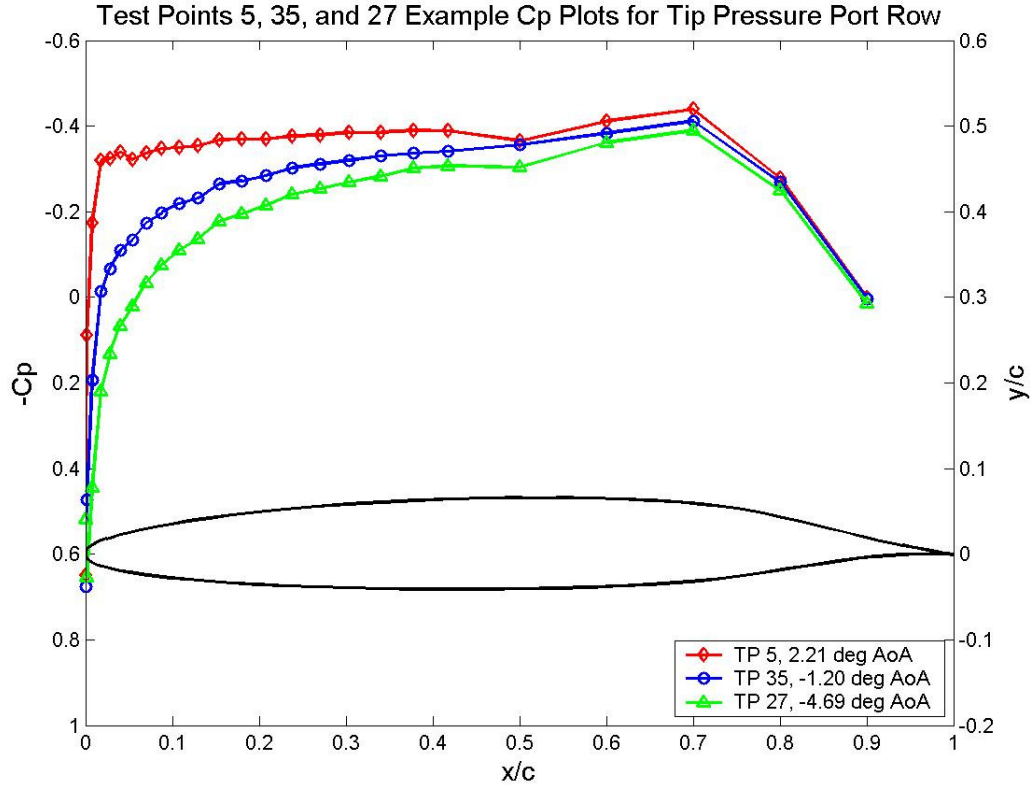
Figure 5: C_p data for tip pressure row at three different *AoAs*

Two test points were compared with the CFD work, one at -2.6°, and the other at -4.7°. These test points showed very good agreement between experimental and computational results, as seen in Figure 6 through 9.
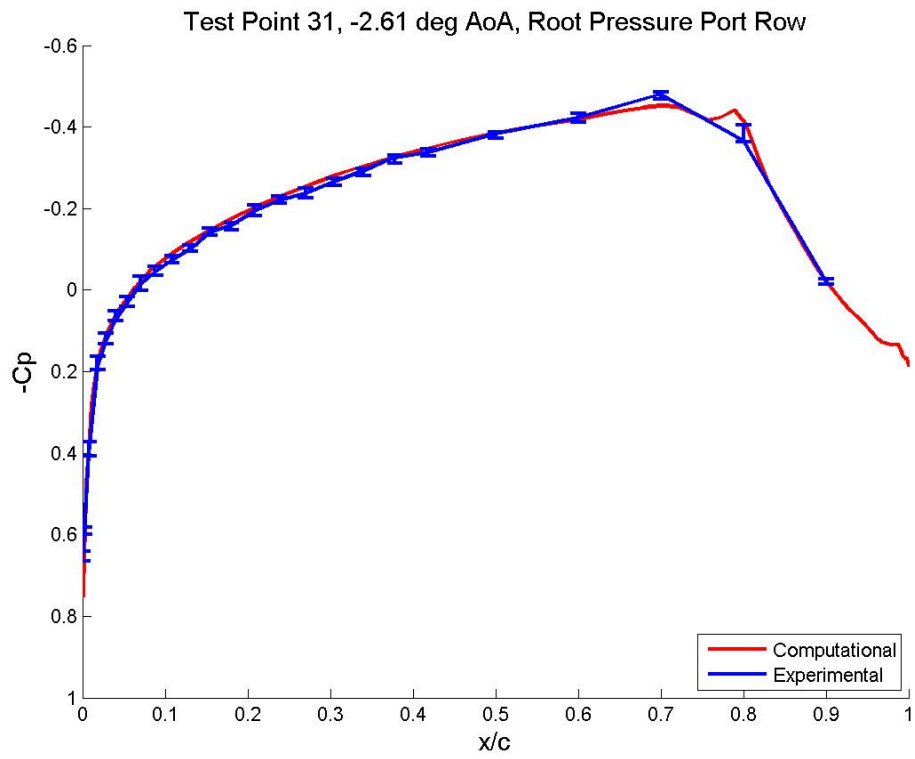
Figure 6: Root pressure port row C_p distribution at AoA = -2.6°
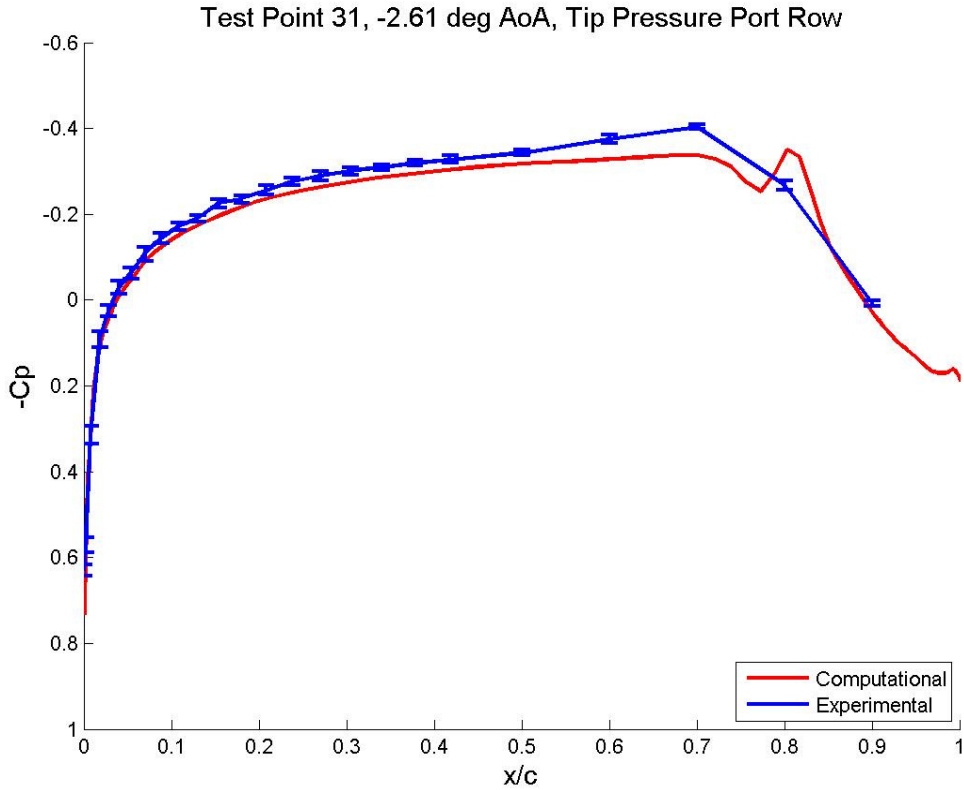
Figure 7: Tip pressure port row C_p distribution at AoA = -2.6°
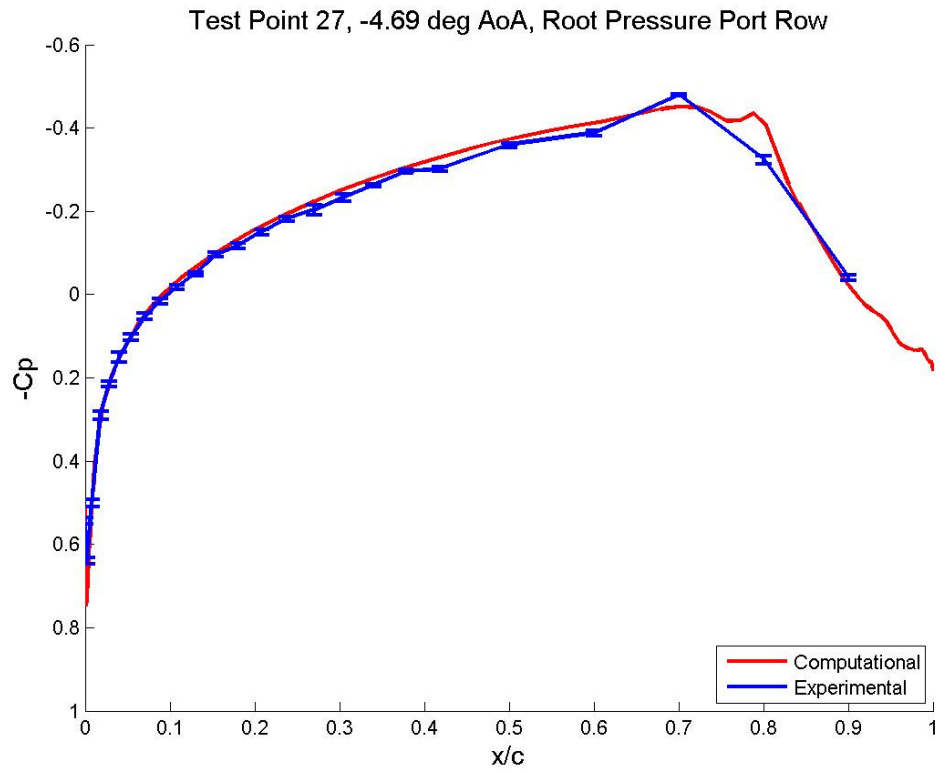
Figure 8: Root pressure port row C_p distribution at AoA = -4.7°
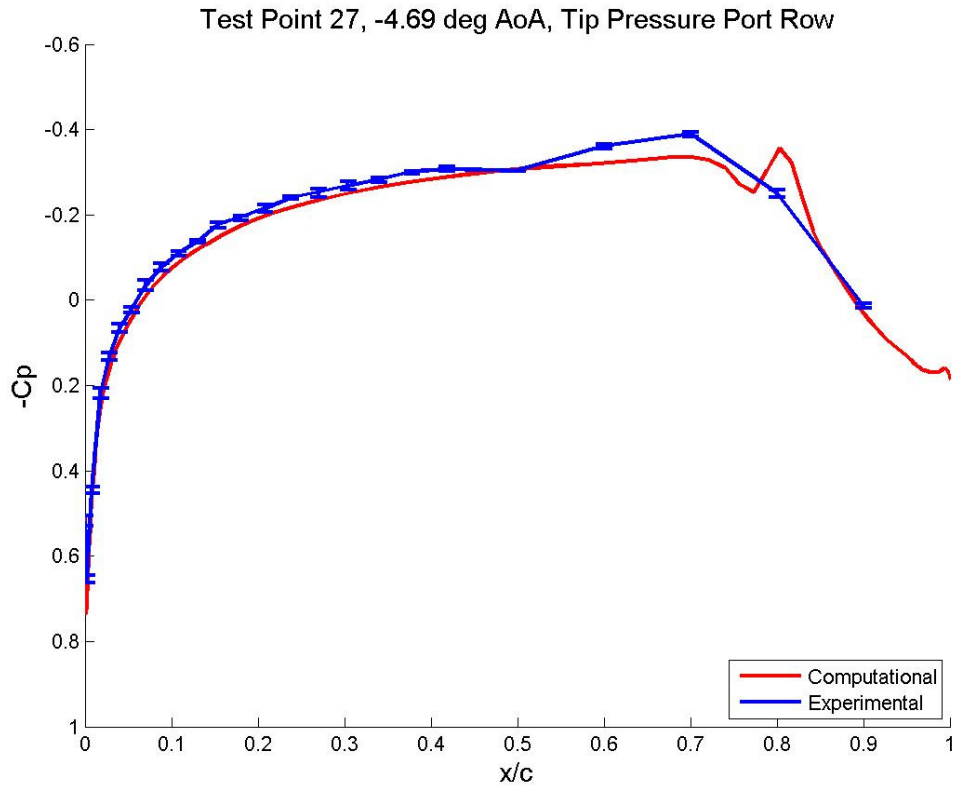
Figure 9: Tip pressure port row C_p distribution at $AoA = -4.7°$

A comparison between the root and tip pressure ports was also completed. These data show a difference in C_p distribution between the root and the tip (as seen in Figures 10 and 11), which was taken into consideration by placing the DREs at the calculated neutral point, which varied along the span of the model.
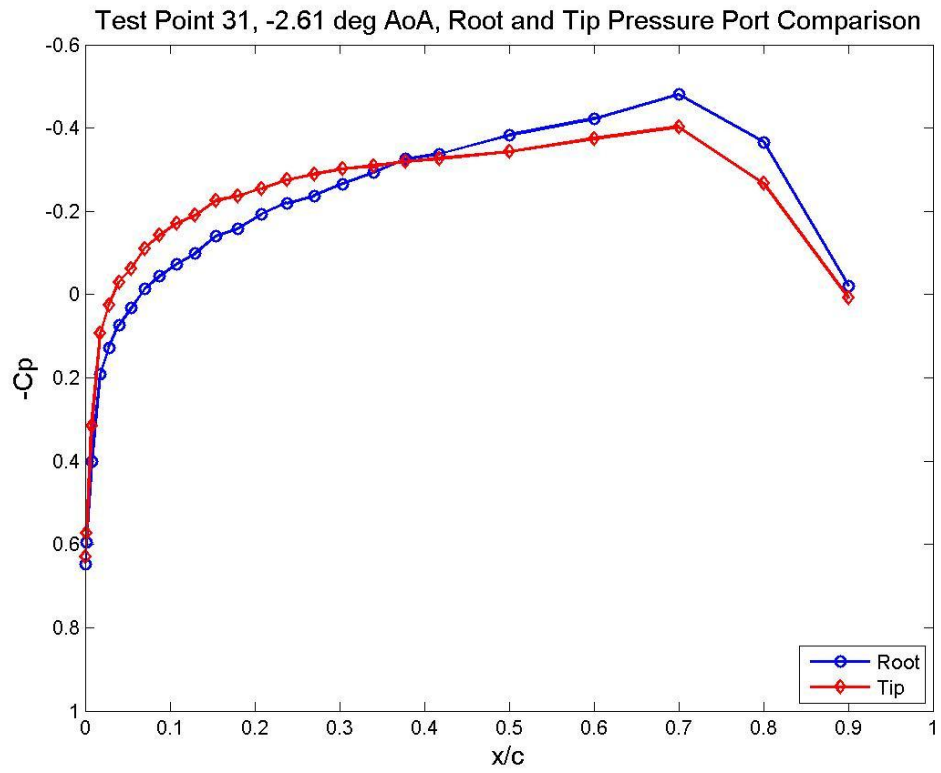
Figure 10: Root and tip C_p comparison at $AoA = -2.61°$
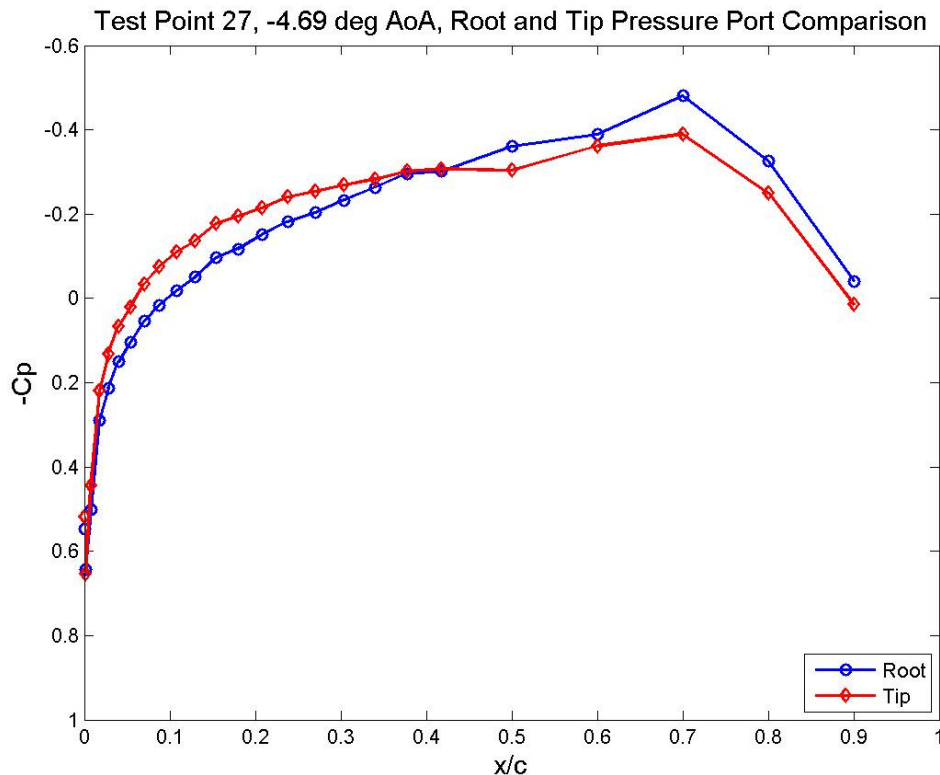
Figure 11: Root and tip C_p comparison at AoA = -4.69°

RECEPTIVITY MEASUREMENTS AT 34% *x/c*

Prior to installing the hotfilm array at 15.4% *x/c*, an array was tested at 34% *x/c*. This

work was in the saturated region of crossflow, and was partly a feasibility study of

detecting crossflow amplitudes with a hotfilm array. Also detailed in Carpenter is the

procedure for calibrating the hotfilm sensors, including temperature compensation.

Because the temperature is changing during the data collection during the dive, there is a

hysteresis loop with the hotfilm voltages. Carpenter solved this hysteresis loop using

Radeztsky *et al*. (1993), in which the hotfilm voltage is linearly dependant on
temperature. A slope for each hotfilm channel is calculated and applied to the hotfilm
voltages. Once this temperature compensation is applied, the hysteresis loop is removed.
Figure 12 shows the raw hotfilm data, and Figure 13 shows the data after it has been
compensated for.
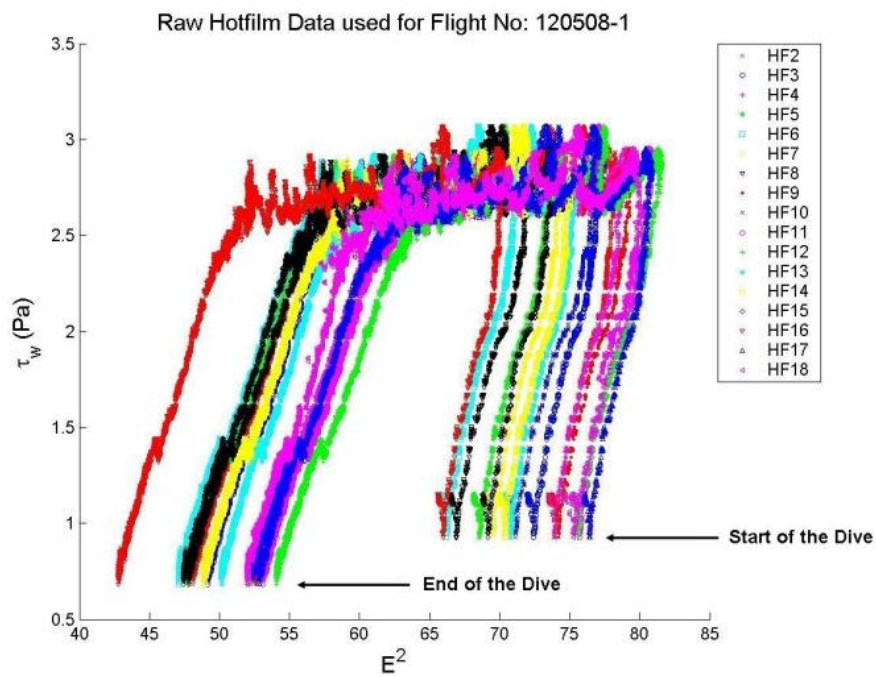
Figure 12: Raw hotfilm data
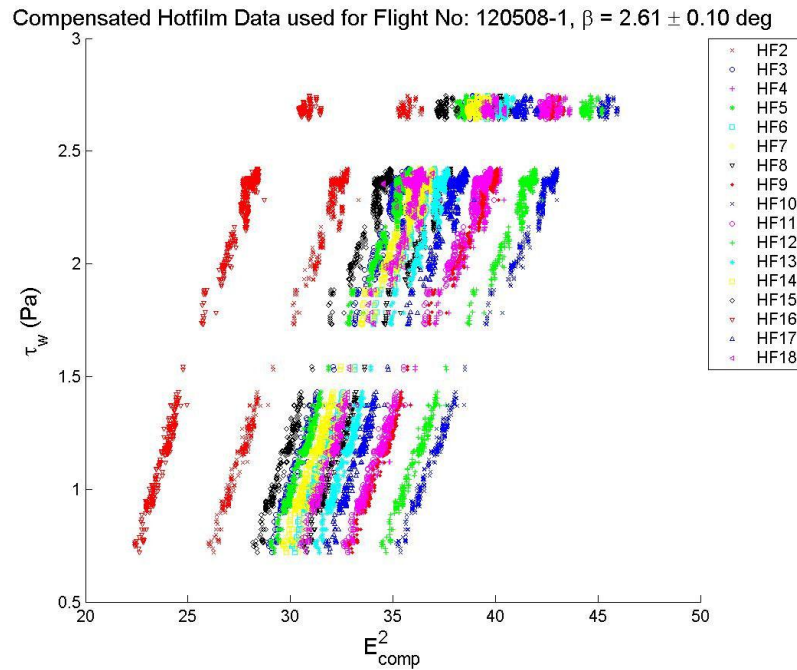
Figure 13: Temperature compensated hotfilm data

The calibration used in Carpenter is derived from Bellhouse & Schultz (1966). The shear stress can be related to the output voltage of the anemometer by a third order polynomial (as seen in Figure 14), after the voltage has been temperature compensated. These calibration curves are derived from data which is within $\pm 0.1°$ of the test angle of attack, and while the pneumatic DREs are not activated. This condition is met during the initial acceleration and final deceleration before the dive, and during the calibrations during the flight.
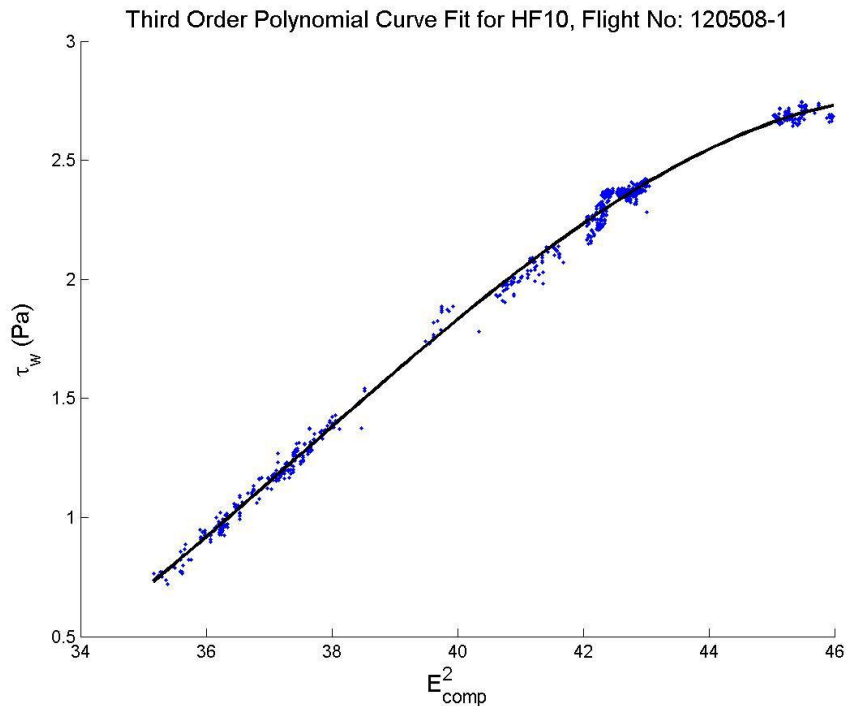
Figure 14: Calibration curve for a single hotfilm channel

Two angles of attack were tested in this initial phase, -2.6° and -4.7°. At -2.6°, it was found that there is very little crossflow growth, potentially because at 34% chord, the crossflow has not had time to grow enough to be detected by the hotfilm sensors. However, at -4.7°, the crossflow can be clearly seen, both with and without the pneumatic DREs. This structure shows the 4.5 mm spacing of the crossflow, and also shows that there is crossflow coming from the pneumatic DREs even when they are not pressurized, due to residual pressure in the chamber from the pressure regulator. These results can be seen in Figure 15.
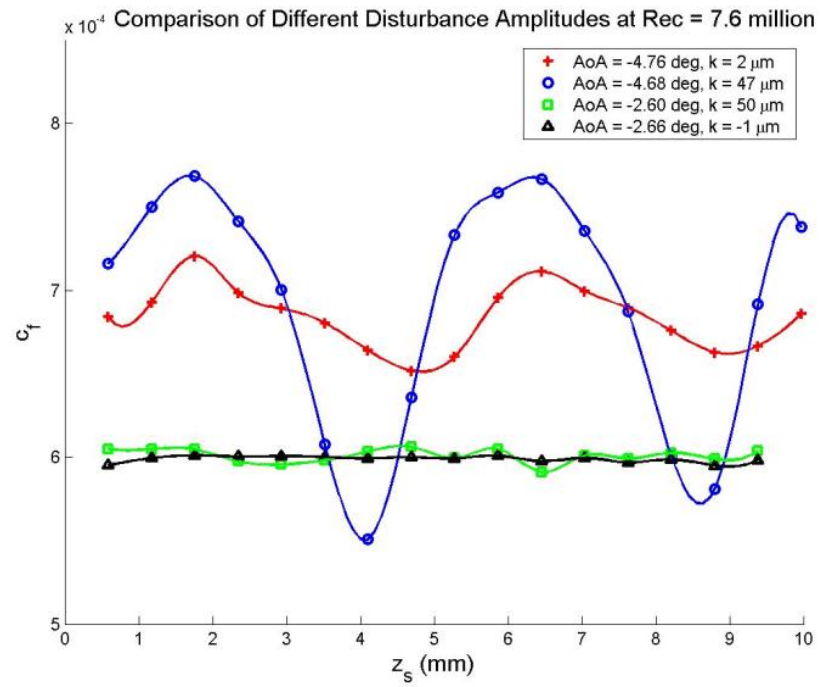
Figure 15: Crossflow amplitudes with a hotfilm array at 34% *x/c*

CHAPTER II

EXPERIMENTAL SETUP

TEST PLATFORM

The 1968 Cessna O-2A Skymaster (seen in Figure 16) that was used for this series of flight tests was chosen primarily for the hard points on the wings upon which test airfoils were mounted out of the propeller wash. The aircraft has sufficient payload capacity for three people (pilot, safety observer, and flight test engineer), twenty channels of anemometry, flight-conditions instrumentation, data-acquisition equipment, test airfoil, and fuel for a one-hour flight plus reserves. The O-2 also adds numerous safety aspects to the flight. One of these is the push-pull configuration of the engines. If one engine were to lose power in flight, there is no yaw to overcome from the single engine still running and the aircraft is able to maintain a safe altitude above ground. Since it was used as an observation aircraft, there is superb visibility to better aid in looking for traffic.

Figure 16: 1968 Cessna O-2A – N630AM

Instrumentation racks have been installed into the rear of the cabin in order to facilitate the flight testing, as seen in Figure 17. A pure sine-wave inverter supplies power to data-acquisition systems, all instrumentation, and a data recording laptop. The instrumentation racks also provide an easy way to interchange instrumentation for different research missions. The standard rack size provides easy mounting for almost any instrumentation module available.
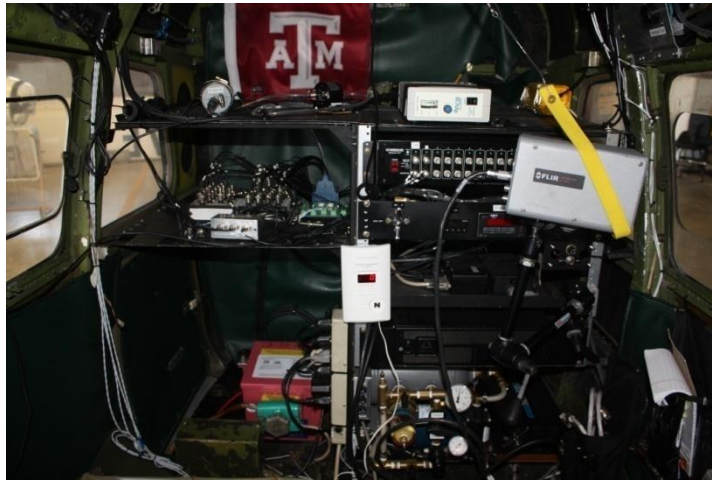
Figure 17: Instrumentation rack

A typical flight profile begins with a climb to 10,500 feet, followed by collecting hotfilm

voltage data at a constant altitude and different airspeeds for shear stress calibration.

Once this is complete, there is a dive at 175 *KIAS* from 10,500 feet down to

approximately 3,000 feet. This speed and altitude range allows approximately two

minutes of conditions at chord Reynolds number, Re_c, of 7.5×10^6. Upon leveling off,

another data collection is performed at a constant altitude and different airspeeds in order

to obtain another calibration at a different temperature for temperature compensation.

Two different test areas are utilized for flights. These test areas are in between victor

airways and away from populated areas in order to minimize the risk of an encounter

with another aircraft. During the flight, air traffic control is contacted to obtain *flight*

following, which allows for another safety factor in avoiding other aircraft. Each of the

test areas has alternate airports that could be used in case of an emergency. The main test area that was used can be seen in Figure 18. College Station can be seen in the lower right of the figure circled in red.
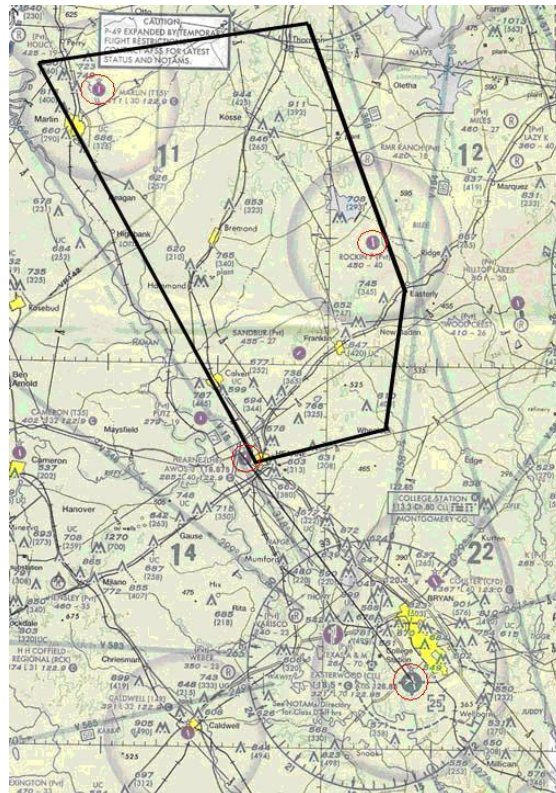
Figure 18: Test area 2

The crew for each flight includes the pilot, a co-pilot/safety observer, and a flight test engineer. During the dive, the pilot is focused on the instruments to maintain a constant flight condition, and the FTE focused on the laptop, so the safety observer is looking

outside the aircraft to make sure there is no other traffic in the area. Moreover, one or more ground personnel are part of the flight operations. They are responsible for making sure nothing appears out of place on the exterior of the aircraft during start and taxi and maintain radio contact with the flight crew during flight operations.

TEST AIRFOIL

The Swept Wing In Flight Testing (SWIFT) model used for these series of tests is a 30° swept wing with a laminar flow airfoil custom designed at Texas A&M. The pressure minimum on the airfoil is at 70% chord, and it does not have any concave structure, so it is ideal for studying the crossflow instability. The model can be seen in Figure 19 along with the *Cp* distribution in Figure 20.

Figure 19: SWIFT model in flight
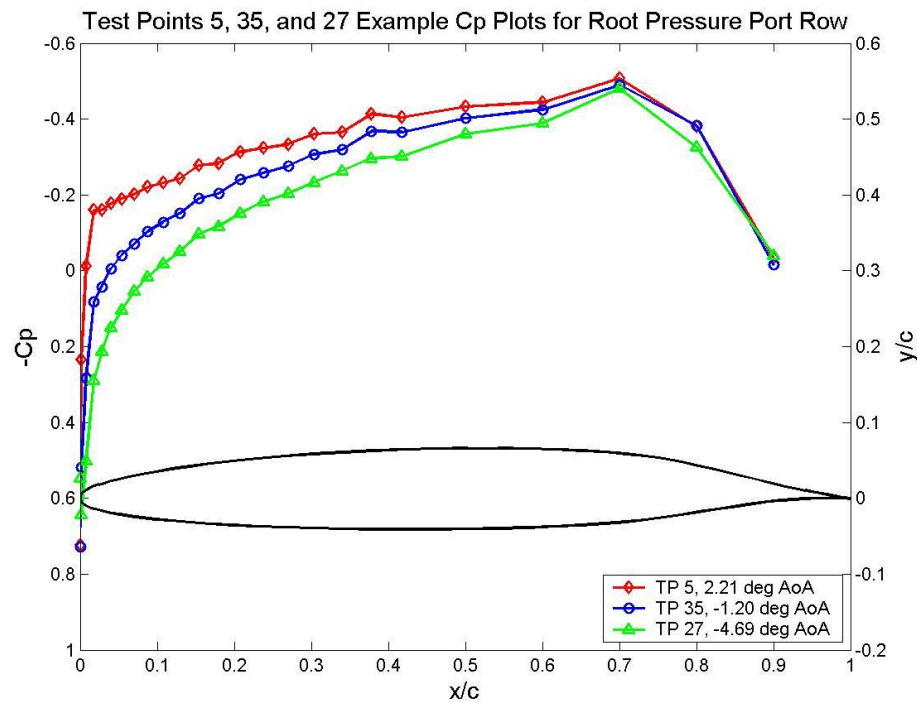
Figure 20: Suction-side pressure coefficient distribution

The airfoil is a precision-machined shell of aluminum, with two halves for the main

section of the airfoil, and an interchangeable leading edge, as seen in the exploded view

in Figure 21. The shelled interior saves weight and is used for instrumentation, such as

pressure transducers. Two leading edges are available – the polished leading edge with

pneumatic insert used for this series of tests, and a painted leading edge that is used for

laminar flow control research.
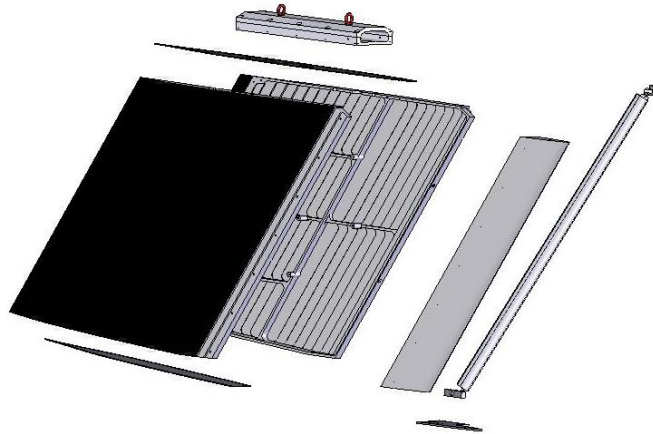
Figure 21: Exploded model view

HOTFILM ARRAY DESIGN AND PLACEMENT

The hotfilm array used was custom designed by Texas A&M and built by Tao Systems.

This specific array is designed with minimum spacing and a sensor length of 500 μm in

order to obtain the highest possible resolution. The array is designed to have

approximately 9 sensors per one wavelength of the crossflow wave being measured.

Because of the inclination of the stationary crossflow wave, the array is oriented at 42°

with respect to the freestream, rather than matching the 30° sweep of the leading edge.

At the same time, the difference in chord location between the first and last sensor is

negligible, and can be ignored. The design of the array can be seen in Figure 22.
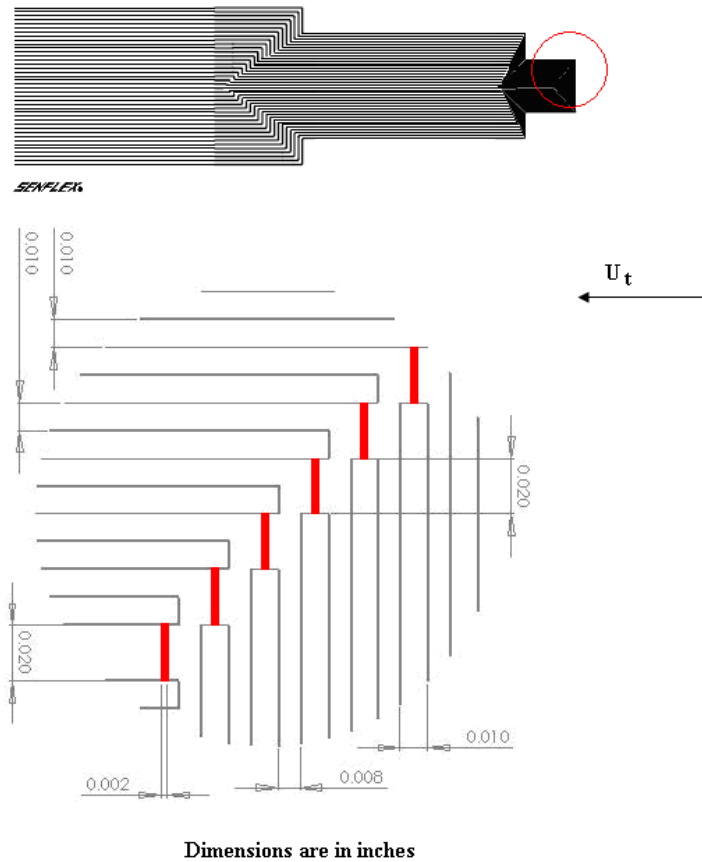
Figure 22: Hotfilm array layout and dimensions

The hotfilm array was applied to the wing at 15.4% *x/c*, which is the location of the

farthest forward static port available on the model. Along with the array, a 320 μm

diameter Preston tube and T-type thermocouple are applied along the same chord line,

but with enough spacing that there is no interference in the flow between the sensors.

This setup provides the Preston tube shear stress reference, static port reference, and

temperature for the calibration of the hotfilm voltages, all at the same chord location on the airfoil, as seen in Figures 23 and 24.
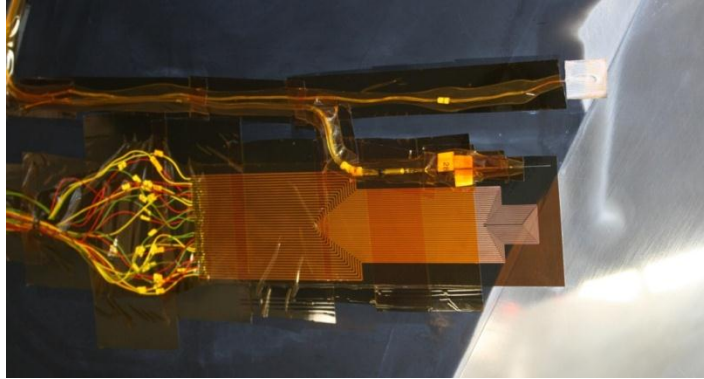
Figure 23: Hotfilm array at 15.4% chord with Preston tube, static port, and thermocouple
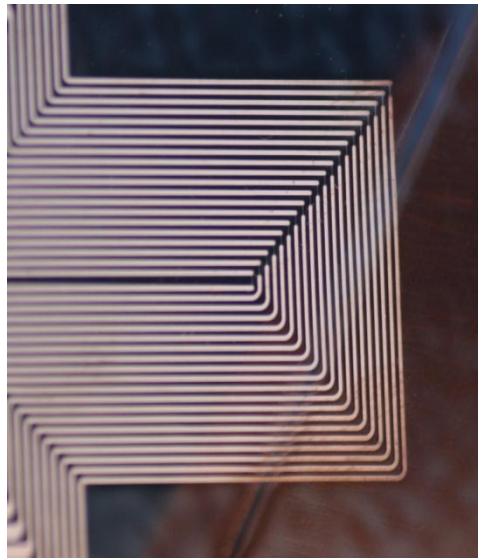
Figure 24: Hotfilm array sensors applied to the airfoil

The anemometers used for the hotfilm array are A.A. Systems AN-1003 units with ten channels each. Each of these units is 50 pounds, and therefore the O-2 is limited to carrying twenty channels without reducing the flight time. The anemometers are installed next to the flight test engineer's seat, where each channel can be adjusted easily, as seen in Figure 25.

Figure 25: Anemometer installed in the aircraft

INSTRUMENTATION AND DATA ACQUISITION

The airfoil model is instrumented with a five-hole probe (seen in Figure 26) and an RTD temperature sensor on the wing of the aircraft. The five-hole probe measures local pitch angle, α, and yaw angle, β, which is translated to model sweep angle, Λ, and model angle-of-attack, AoA. Static pressure, p, and dynamic pressure, q, are also measured.

Using these data, the altitude, Mach number, true airspeed, and chord Reynolds number are calculated and recorded.

Figure 26: Five-hole probe attached to the SWIFT model

There are two displays for the pilot on the instrument panel of the aircraft. One shows Re_c of the airfoil, while the other shows the *AoA* of the model. These values are displayed in real time, updating continuously. Using these displays, the pilot is able to keep constant flight conditions throughout the duration of the testing.

Figure 27: Re_c and β display

In conjunction with the two main displays seen in Figure 27, a small LCD screen is

mounted on the yoke of the aircraft to show more information to the pilot as seen in

Figure 28. This display offers slider representations of Re_c and β, along with derivatives

of each to provide the pilot with more information. Using this information, the pilot is

able to keep control of the flight conditions much better than just the digital display.

Figure 28: LCD display

All data are recorded in flight in real time by a laptop controlled by the flight test

engineer. A Labview program is used that can simultaneously record parameters and

display essential parameters for the FTE to monitor. The laptop acquires the signals

through three National Instruments DAQ boards – a PCI-6071E, a PCI-6723, and a

USB-9211A. The 6071 is used as the primary input board, with enough analog inputs to

record the hotfilm voltages and all air data parameters with a 12-bit resolution. The 6723

is used to output the Re_c and β values to the pilot display with a 13-bit resolution. The

9211 is a thermocouple input board, which monitors four different thermocouples in and

on the SWIFT model with a resolution of 24 bits.

MEASUREMENT UNCERTAINTY

Four Honeywell Sensotech FP2000 pressure transducers were used to measure the

parameters from the five-hole probe, three differential for α, β, and q, and one absolute

for p. The differential transducers were all ±2 psid with an accuracy of 0.002 psid. The

absolute transducer had a maximum pressure of 15 psia with an accuracy of 0.015 psia.

The pressure transducers provided a greater accuracy than was possible to align the

probe with the airfoil, so the overall uncertainty in model AoA and Λ was determined by

the alignment procedure. Despite best efforts in the alignment procedure, the accuracy of

the alignment for AoA is estimated to be ±0.2°, while the accuracy of Λ is ±0.1°. These

uncertainties are only introduced when the five-hole probe is removed and replaced on

the model, so all flights in this set of experiments have the same uncertainty, and are

directly comparable.

Two Honeywell Sensotech FP2000 pressure transducers were used to measure the

Preston tube parameters, one absolute gauge connected to the static port on the model,

and one differential between the Preston tube total pressure and the static port pressure.

These transducers have the same accuracy of the five-hole probe transducers.

PNEUMATIC DREs

In order to excite the crossflow, a system to vary the height of a row of spanwise-

periodic discrete roughness elements (DRE) was used. The system is made up of a

chamber with 2 mm diameter holes on 4.5 mm centers along approximately 2% x/c

covered with a polyester tape, as seen in Figure 29. The chamber is then pressurized

from a tank in the cabin of the aircraft. Before the system is installed in the airfoil, a

confocal laser is used to calibrate the height of the roughness element with respect to the

differential pressure between the chamber and a static port on the airfoil. Using this

calibration, the height of the roughness element can be measured within 0.1 μm, with a

maximum height of approximately 50 μm. The inflated DREs can be seen in Figure 30.
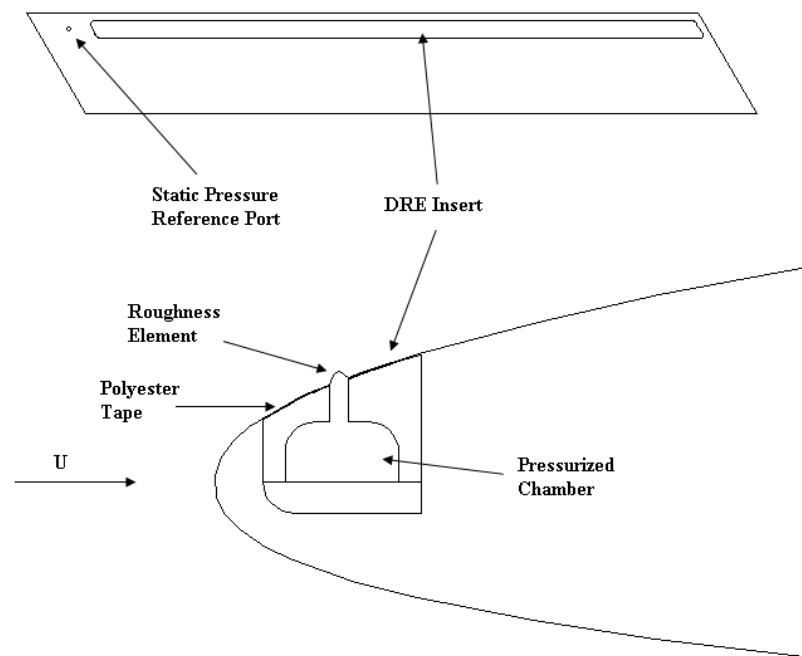

Figure 29: Pneumatic DRE system

Figure 30: Pneumatic DREs

APPLIQUÉ DREs

Appliqué DREs were used in conjunction with the pneumatic DREs to amplify the desired wavelength, but still allowing for a varying of height. These DREs are approximately 6 μm high, and can be printed in any desired distribution and shape. A sample of the DREs can be seen in Figure 31.

Figure 31: Appliqué DREs superposed on pneumatic DREs

Different batches of applique DREs have been measured, and were found to vary

between 6 and 10 µm high. The applique DREs also have a different profile from the

pneumatic DREs, as seen in Figure 32. The appliqué have more of a sharp profile while

the pneumatic DREs have a more rounded distribution of heights. The overall height of

the pneumatic DREs was measured at the top of the profile, in the center of the circle.
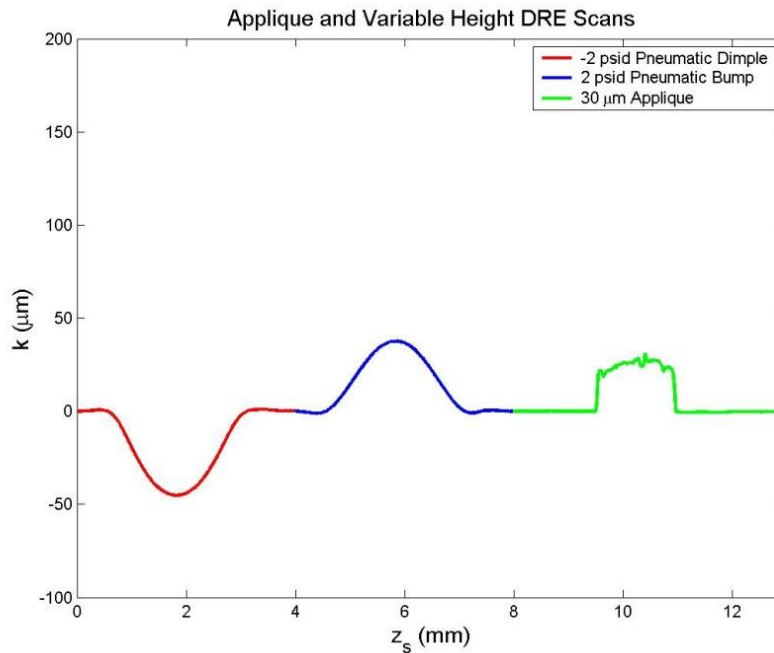
Figure 32: Pneumatic dimple and bump, and applique DRE profiles

VERIFICATION OF FLOW OVER HOTFILM ARRAY

In order to verify that the flow over the hotfilm array is laminar, a FLIR Thermacam

SC3000 Infrared (IR) Camera with a 20° lens is pointed at the array on the airfoil. The

aircraft climbs to 10,500 ft and cold soaks the model for approximately 20 minutes

before initiating at dive at 170 *KIAS* to get to 7.5 million Re_c. During the dive, as the

temperature of the outside air is increasing, the IR camera is able to detect transition

between laminar and turbulent due to the different heat transfer properties of the flow.

As can be seen in Figure 33, the flow over the front of the hotfilm array is laminar.

There are turbulent wedges created by the thermocouple, Kapton tape on the hotfilm

array behind the sensors, and a wedge off of the Preston tube. None of these wedges
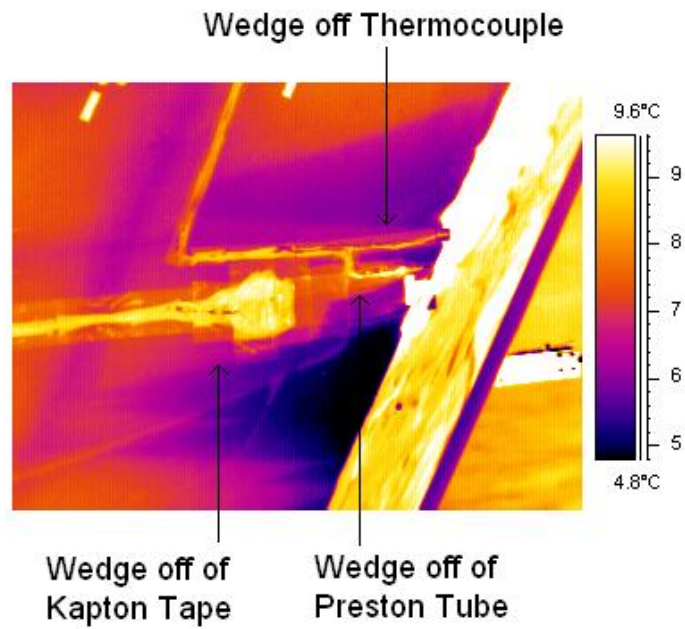
interfere with the array.

Figure 33: IR image of hotfilm array

CHAPTER III

THEORY

INSTABILITIES

There are four main types of instabilities that can cause transition to turbulence –

crossflow, Tollmien-Schlichting waves, Görtler vortices, and attachment line

contamination. Attachment line contamination can be easily controlled by keeping the

leading edge radius below a critical value (Pfenninger 1977). Görtler vortices are

destabilized in boundary layer flows by concave curvature (Saric 1994), and can be

avoided by choosing an appropriate airfoil profile. T-S waves can be controlled by a

favorable pressure gradient. Crossflow is destabilized by a favorable pressure gradient,

and is therefore the last big hurdle in laminar flow control (Saric & Reed 2003).

CROSSFLOW AND ROUGHNESS

Radeztsky *et al*. (1999) gives a good overview of the effect of roughness on crossflow.

Freestream turbulence has a large effect on the type of crossflow seen in transition.

When tested in a high turbulence wind tunnel vs. a low turbulence wind tunnel (Bippes

and Müller 1990; Bippes 1991), the traveling crossflow dominated transition in the high

turbulence environment, while the stationary crossflow dominated the low turbulence

wind tunnel. As flight is a low turbulence environment, the stationary crossflow will

dominate.

Surface finish also had a large effect on transition. Radeztsky *et al*. (1999) started with a painted surface with a RMS roughness of 3.30 μm, and worked towards a highly polished aluminum surface with a RMS roughness of 0.121 μm. The transition location moved significantly back with the polished aluminum surface compared with the painted surface.

The next experiment conducted concerned isolated roughness elements, and their effect on transition. It was found that when roughness elements were placed at or near the neutral stability location of the most unstable waves, it decreased the transition Reynolds number, but had no effect when placed further forward or aft. This indicates that the critical portion of the airfoil is within the first few percent of chord, and any roughness beyond that (within certain bounds) should have little or no effect on transition.

HOTFILM MEASUREMENTS

Multi-element surface-mounted hotfilm sensors are used in a variety of applications of flow sensing. They can be used for transition location detection by analyzing the spectral content of the voltage signal, and also for shock detection. In the past, they have also been used for crossflow vortex identification (Magalan *et al*. 1990, Agarwal *et al*. 1992), but in these instances, only voltages were recorded, not actual shear stress values. Recently, Carpenter *et al*. (2009) developed a calibration scheme using a preston tube, static port and thermocouple in conjunction with the hotfilm sensors. This calibration

also temperature compensates the voltages, as the temperature is continually changing as the aircraft descends in the atmosphere.

CHAPTER IV

RESULTS, DISCUSSION AND CONCLUSIONS

Three different leading edge conditions were tested during this experiment. All three

conditions included the pneumatic DREs in varying heights, but all had different

appliqué DREs applied to the leading edge. Initially, just the pneumatic DREs were

tested, but it was found that a 2.25 mm wave was dominating over the 4.5 mm wave of

the pneumatic DREs. Different amplitudes of circular appliqué DREs were superposed

on the pneumatic DREs and tested with no excitation of the 4.5 mm wave. Finally, an

array of elongated DREs was applied, and successfully excited the 4.5 mm wavelength.

TEST CONDITIONS

All flights were conducted at the same test conditions, with an AoA = -4.7° and a Re_c =

$7.5x10^6$. These conditions promoted strong crossflow growth as compared to higher

AoA. Seen in Figures 34 and 35 are two charts comparing N-factors of the control and

critical wavelength of crossflow being studied at two different AoA. As can be seen, the

lower angle of attack has higher N-factors, indicating more crossflow growth.
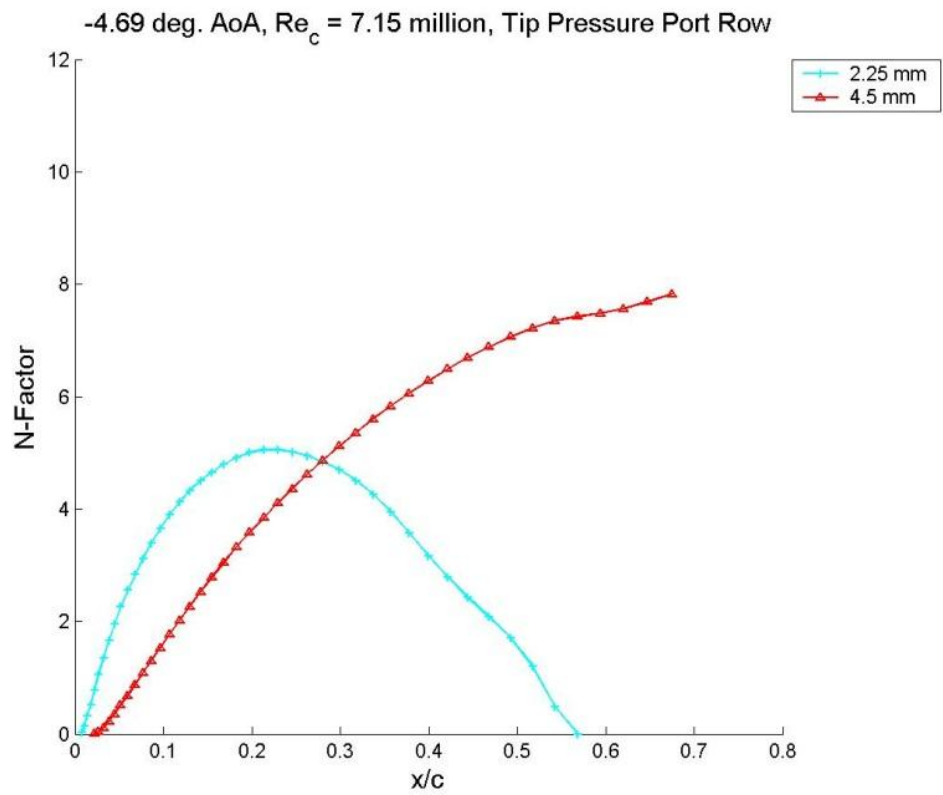
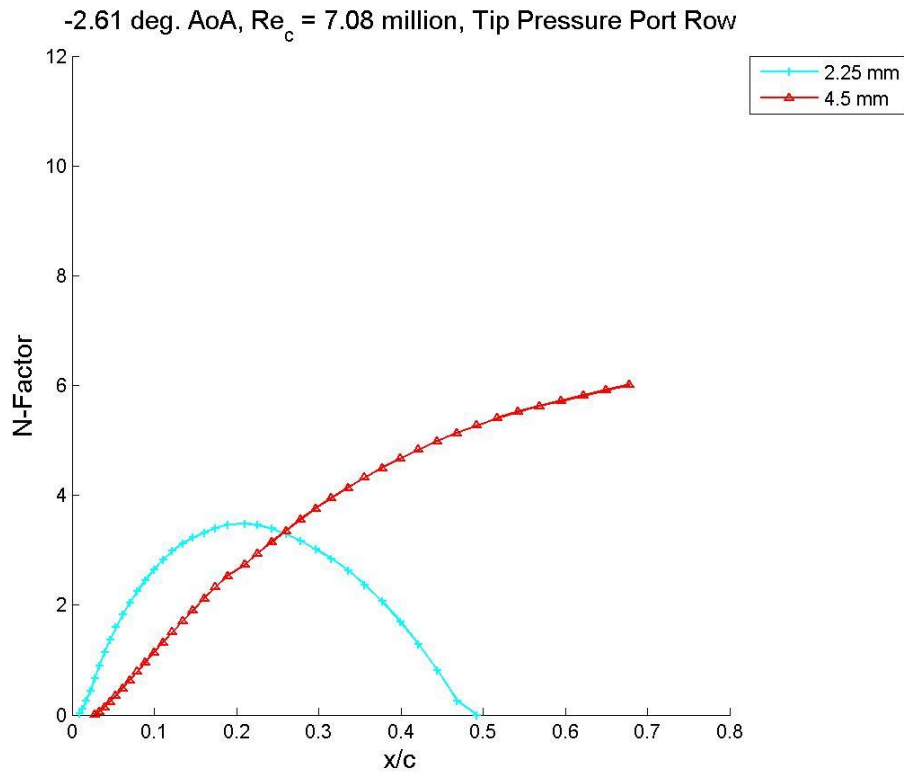Figure 34: N-factors for $Re_c = 7.1 \times 10^6$ and $AoA = -4.7°$

Figure 35: N-factors for $Re_c = 7.1\text{x}10^6$ and $AoA = -2.6°$

During the duration of collecting data, the pneumatic DREs are able to be continually

adjusted in height. The initial flights were conducted with steps of approximately 15-20

µm, going up to a maximum of 45 µm. A typical DRE height profile can be seen in

Figure 36. The final three flights were each flown at a different height through the dive –

20 µm, 35 µm, and 45 µm – in order to find an average over the entire range of the dive,

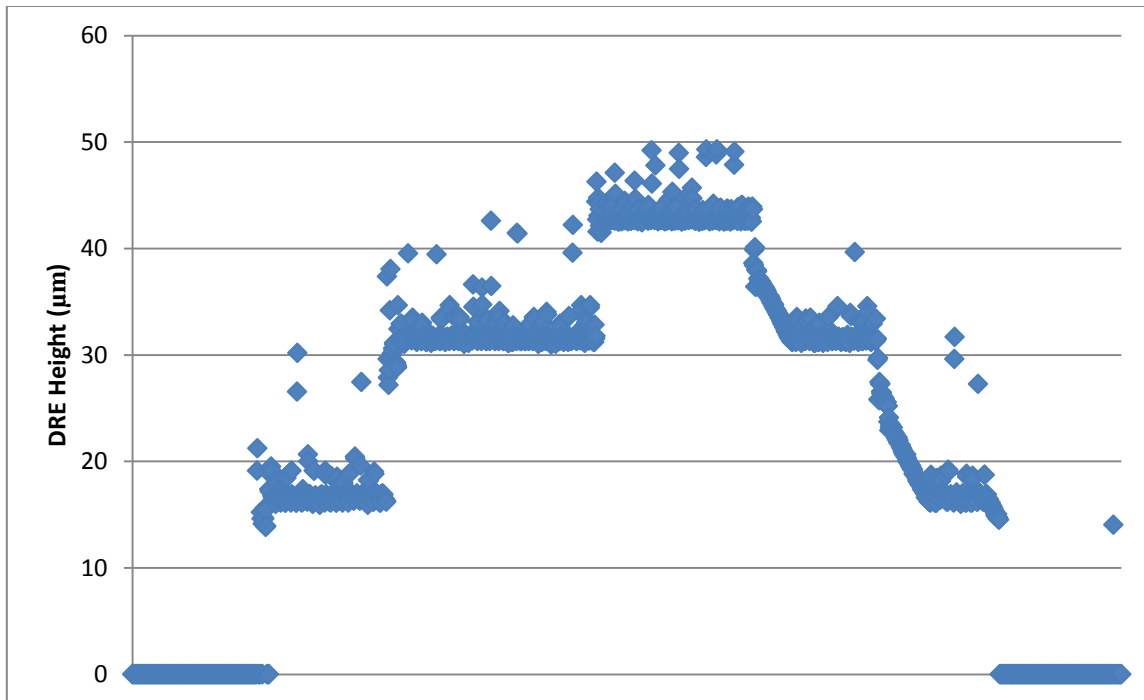and to determine the effect on shear stress by the freestream conditions.

Figure 36: Typical DRE height during a flight

PNEUMATIC DREs ONLY

The first flights were conducted with pneumatic DREs only. The results from these flights were dominated by a 2.25 mm wave (as seen in Figure 37), which was thought to be coming from a different row of pneumatic holes at the 2.25 mm wavelength that had been plugged with epoxy, but still created a small non-uniformity on the surface of the leading edge. Based on these results, it was decided to add appliqué DREs to the surface of the pneumatic DREs to amplify the desired wavelength.
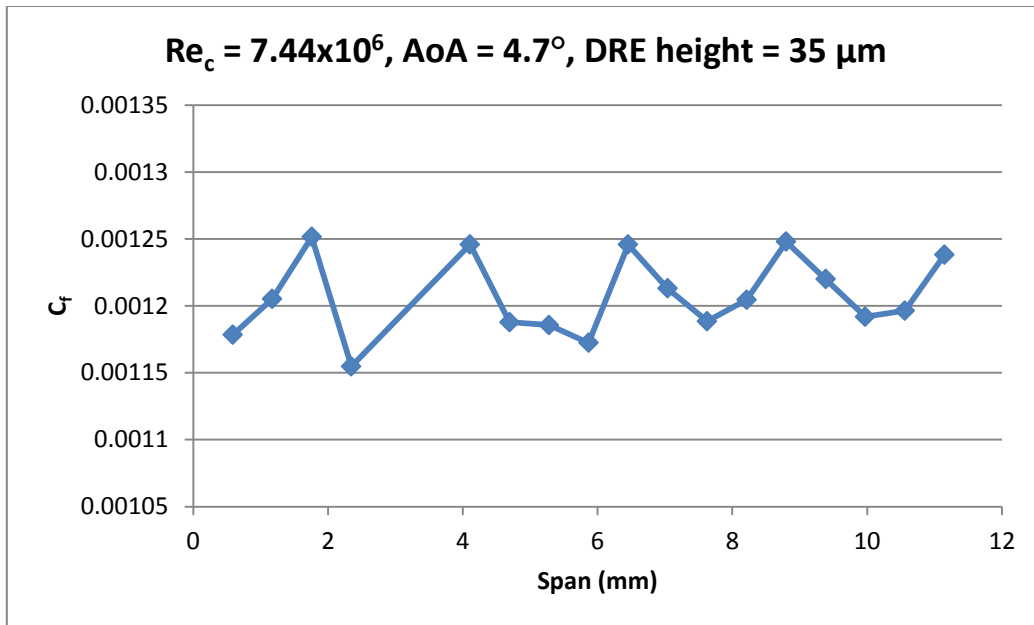
Figure 37: C_f distribution with pneumatic DREs only

CIRCULAR APPLIQUÉ DREs

The first attempt at exciting the 4.5 mm wavelength was to apply 1 mm diameter, 6 μm height appliqué DREs over the center of the pneumatic DREs. The results of these flights appeared the same as the previous flights. Both one and two layers of appliqué DREs were attempted, but neither successfully excited the proper wavelength. Seen in Figure 38 is a representative chart of the shear stress distribution along the span with these conditions.
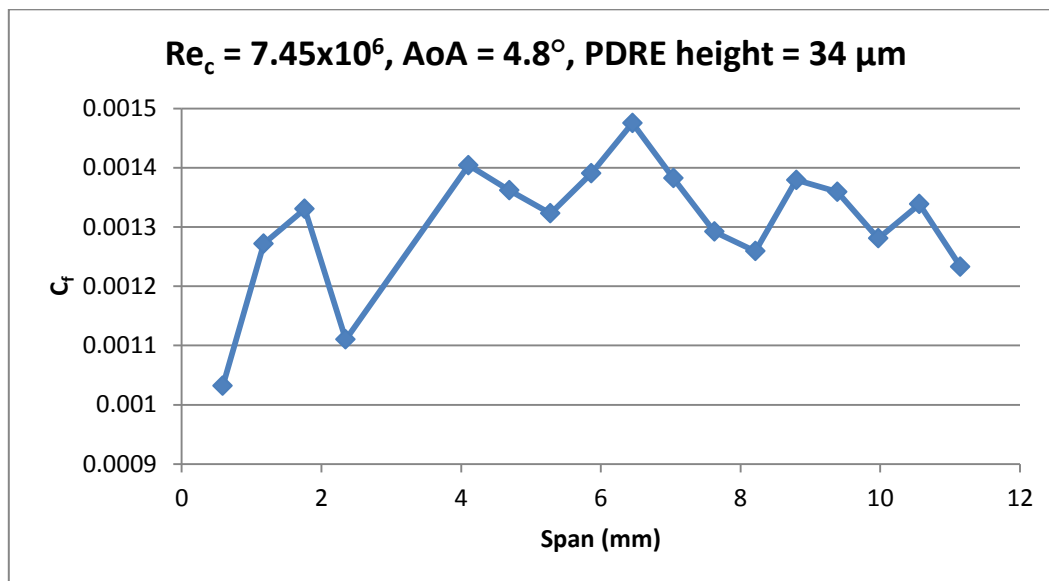

Figure 38: C_f distribution with 10 μm of circular appliqué DRE applied

ELONGATED APPLIQUÉ DREs

Based on Kosinov *et al.* (2009) a potential solution was to apply elongated DREs to the

pneumatic DREs, as seen in Figure 39. The appliqué were tested in increments of 10 µm

(one layer), and with 40 µm applied, a 4.5 mm wave was observed at each increment of

pneumatic inflation as seen in Figure 40. As can be seen, there is still a component of the

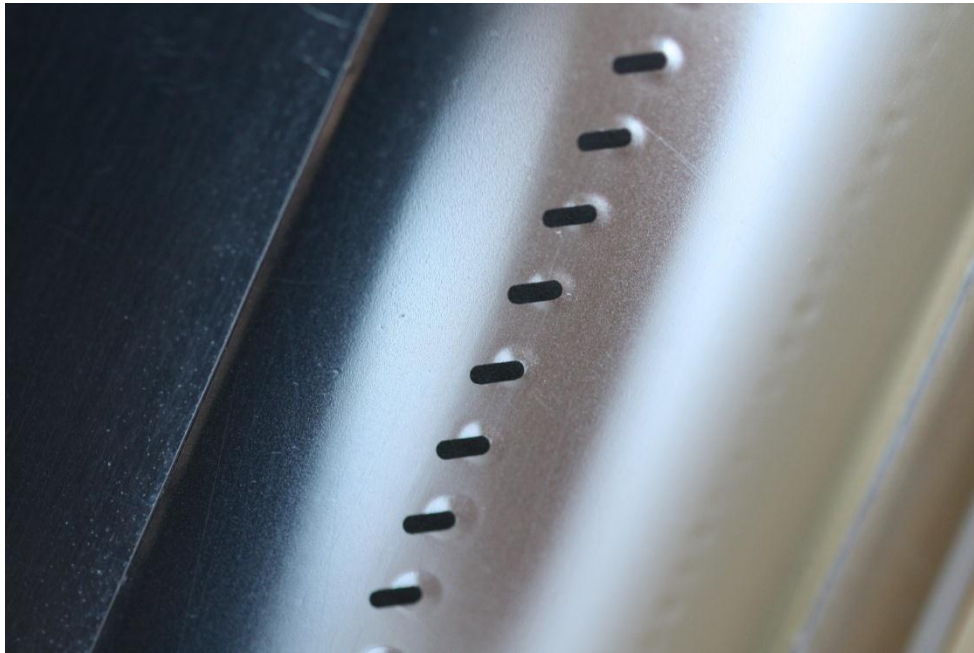2.25 mm wave coming through, but the 4.5 mm wave can be clearly seen and analyzed.

Figure 39: 3 mm x 1 mm appliqué DREs applied to 2 mm diameter pneumatic DREs
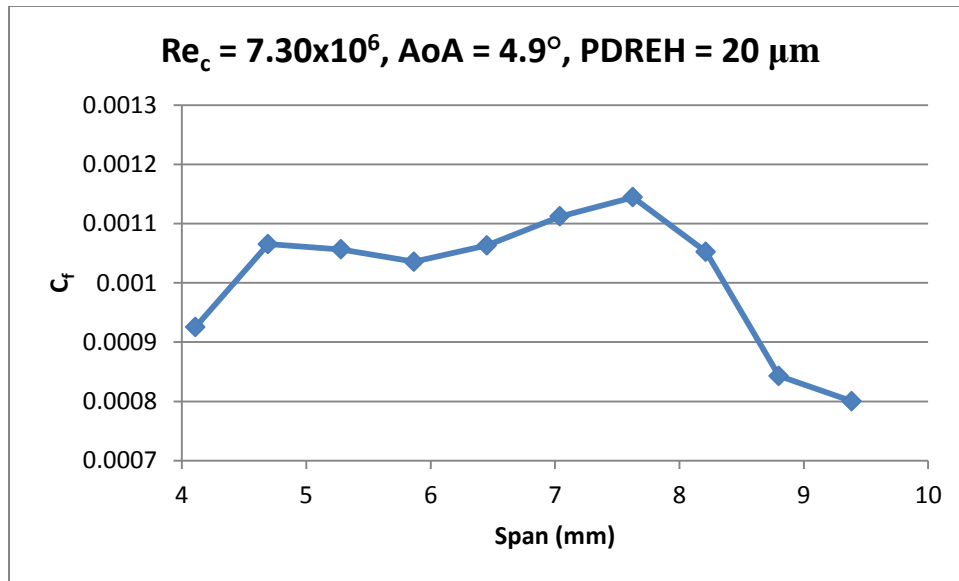
Figure 40: C_f distribution with elongated appliqué DREs

The next step was to fly three flights with three different pneumatic DRE heights in order to fully understand what is happening to the crossflow at 15.4% relative to the pneumatic height.

For each of these flights, the dive data was filtered to be within 0.1° of the target beta, within 1 μm of the target pneumatic DRE height, and above $7.0x10^6$ chord Reynolds number. Once the data were filtered, sections of data that were on condition for more than approximately 5 seconds were analyzed.

SPECTRAL ANALYSIS

During the last flights, one anemometer was not working correctly, so only ten channels of hotfilm voltage were recorded. Because a traditional FFT would not reveal much information on the spectral content of only ten data points, the Lomb method (Press 1992) was used to draw out more information. To obtain a good overall picture of the content of each section of data, the Fourier coefficients were found for each time step, and then averaged to form the final data set of the spectral content.
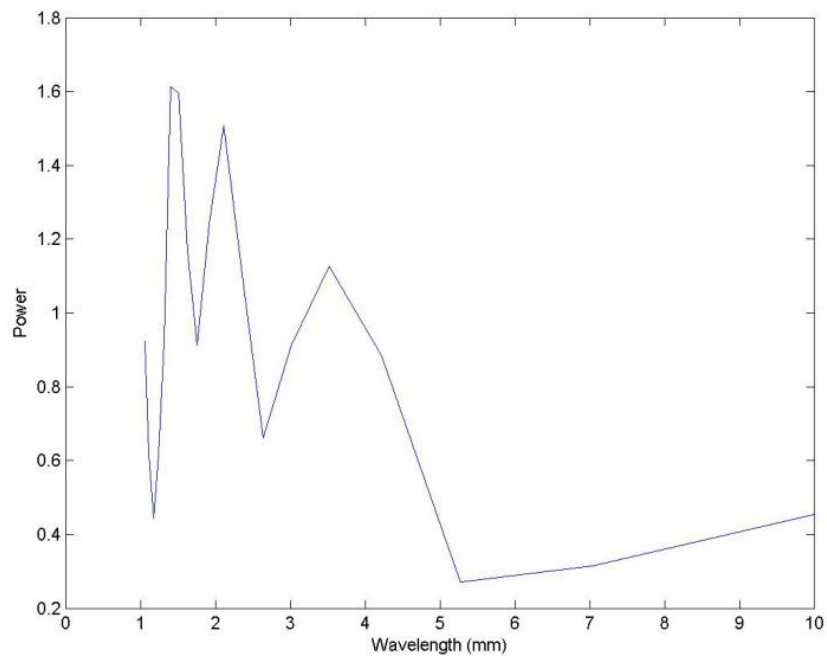
Figure 41: Section 204 – 20 μm pneumatic DRE height

Figure 42: Section 352 – 35 µm pneumatic DRE height
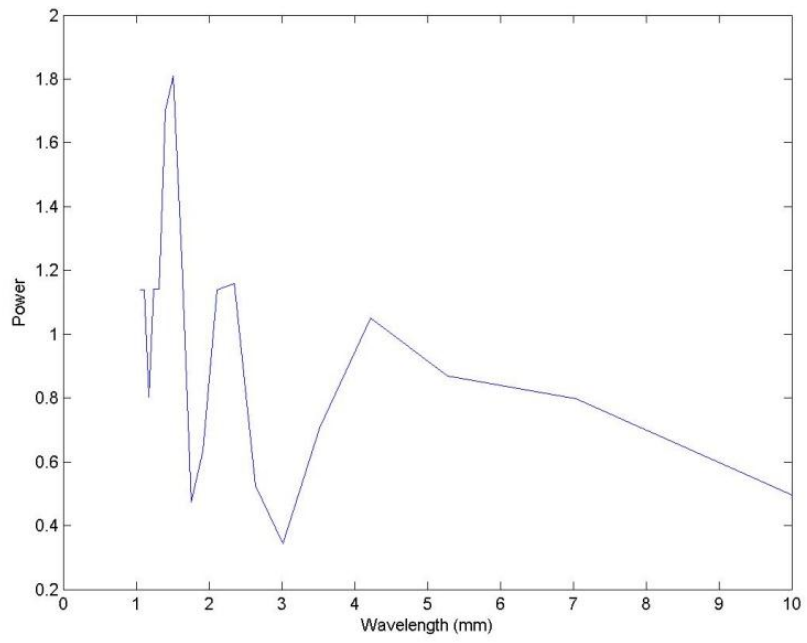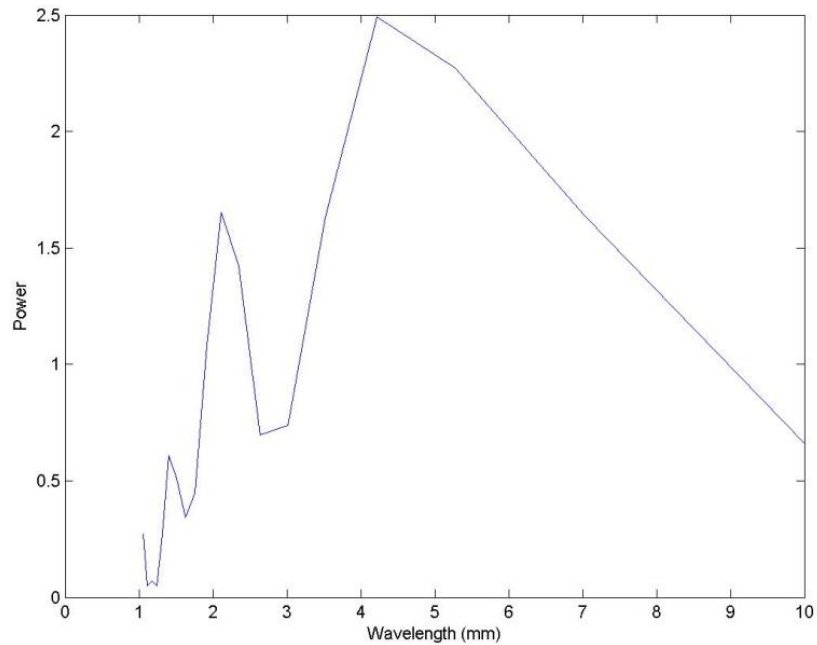
Figure 43: Section 455 – 45 µm pneumatic DRE height

As can be seen in Figures 41 through 43, a 4.5 mm wave is present, along with two of its harmonics - 2.25 mm and 1.125 mm.

RECEPTIVITY

At each different DRE height, the RMS average of the shear stress was calculated and plotted. As can be seen in Figure 44, the shear stress is changing with respect to the input amplitude.
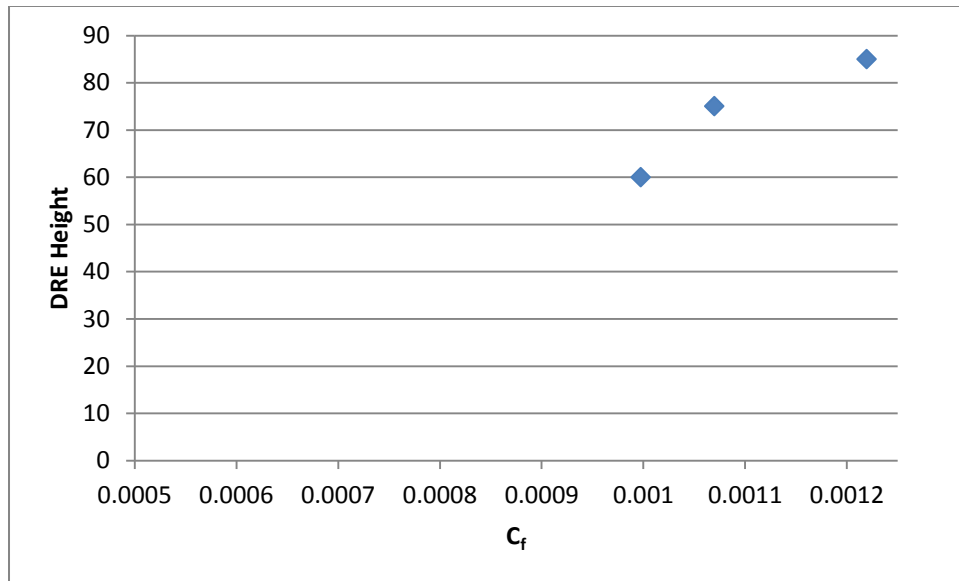
Figure 44: Shear stress at three different DRE heights

Due to the large size of the Preston tube used to calibrate the hotfilms relative to the size of the boundary layer, the value of shear stress is not accurate, but the differences at the same chord location are valid. As can be seen in Figure 45, the shear stress at 34% is saturated, and not dependent on the input amplitude of the pneumatic DREs. In contrast of this, the shear stress at 15.4% is not constant with respect to the input roughness.
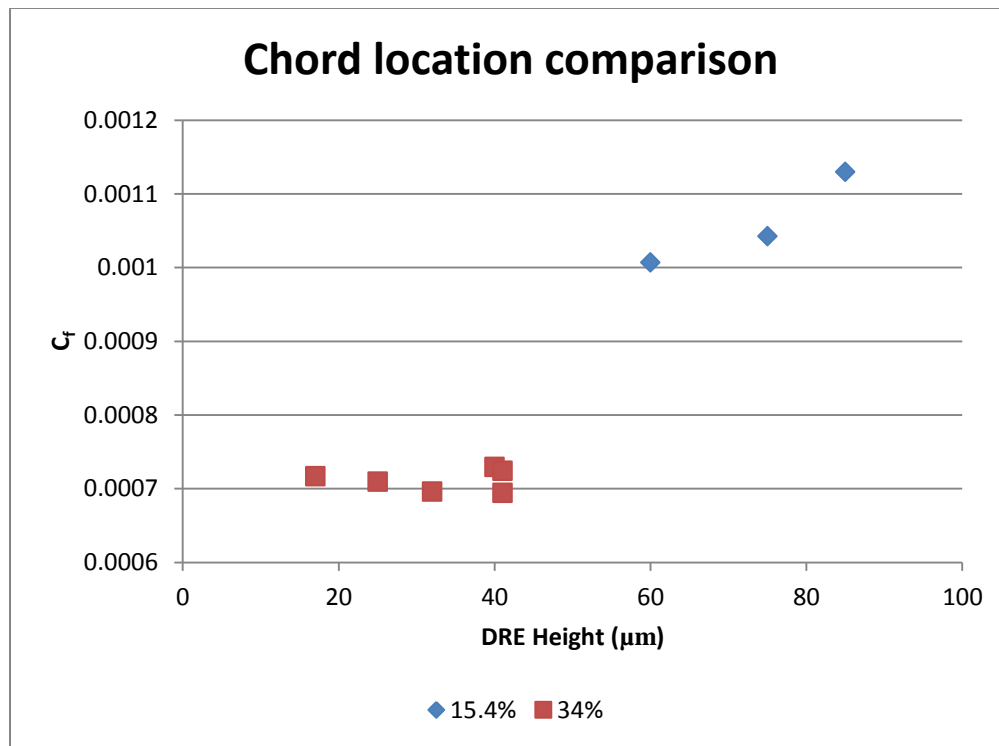
Figure 45: Comparison of 15.4% and 34%

EFFECT OF FREESTREAM CONDITIONS

As the aircraft descends in the atmosphere, the air gets denser, so the pilot slows the aircraft down to maintain a constant Reynolds number. It was noticed that the shear stress as measured by the hotfilms was jumping slightly around with variations in angle of attack and Reynolds number. Figures 46 and 47 compare the RMS C_f with different parameters during flight.

Figure 46: Altitude comparison

Figure 47: True airspeed comparison

The above two figures show a difference over the course of the flight, but due to the resolution of the data, it is not clear what is happening with the shear stress. More work needs to be done to better analyze the effect that freestream conditions have on the sehar stress.
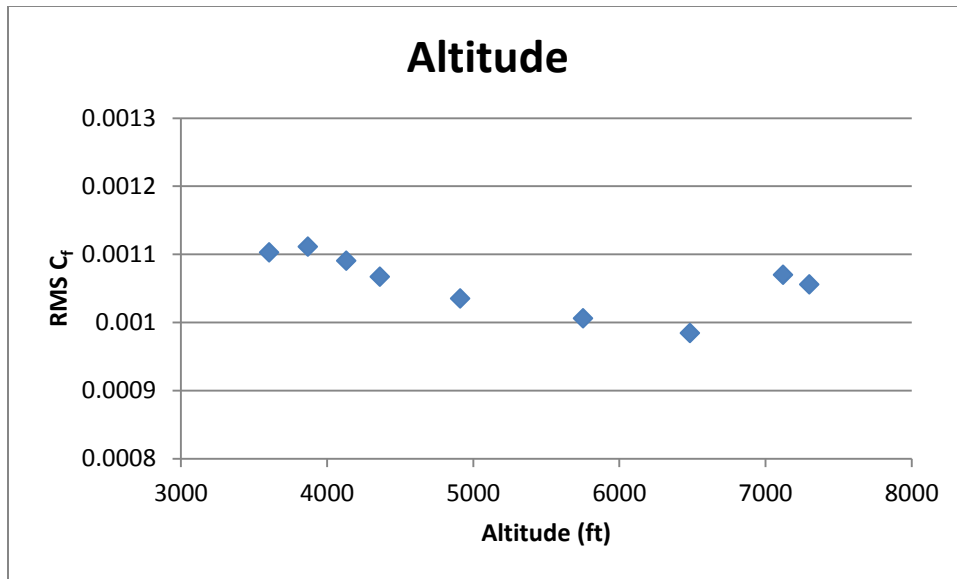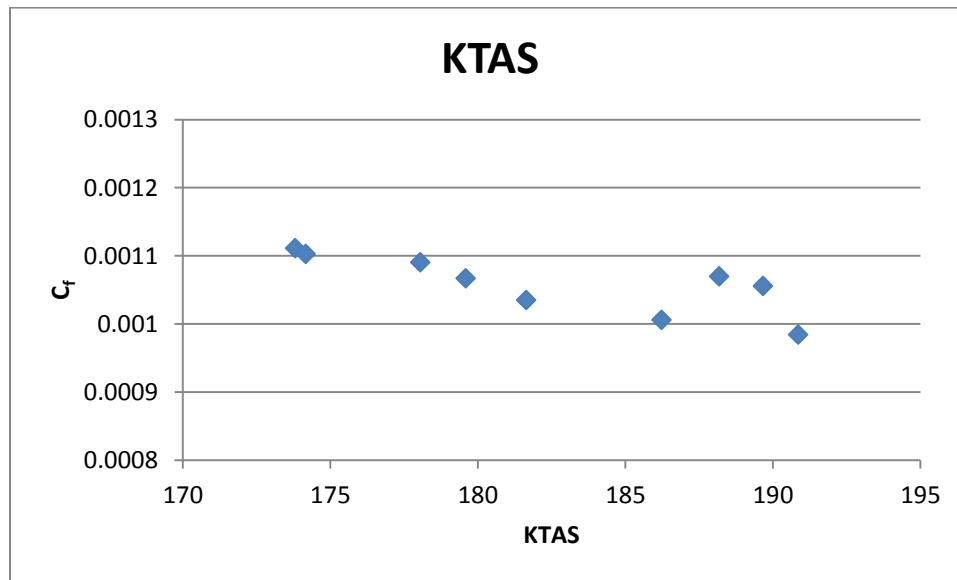
CONCLUSIONS

An experiment was performed to gather data on the relationship between roughness height and crossflow disturbance amplitude. These data were found in flight, in a low-disturbance environment on a natural laminar flow airfoil. This airfoil had periodic roughness placed on the leading edge, and the shear stress from the crossflow off of the roughness was measured with a set of hotfilm gauges placed downstream in the unsaturated region of the disturbance.

It was found that DREs are dependent on the freestream turbulence level on how effective they are. In wind tunnel tests at ASU in the Unsteady Wind Tunnel, it was found that applique and pneumatic DREs were quite effective in delaying transition in a turbulence level of 0.04%. However, when the wind tunnel was moved to Texas A&M, modifications were made to reduce the turbulence level to 0.02%, and with the modification, it was found that the applique DREs were not as effective at delaying transition. In the initial flight tests with the O-2, it was found that the applique DREs were effective at delaying transition, but the pneumatic DREs did almost nothing to the transition location.

More work needs to be done to fully understand what is happening with the shear stress due to the crossflow. Detailed leading edge boundary layer scans are needed from the Klebanoff-Saric Wind Tunnel to determine what is happening at the leading edge. Once that is understood, more flight tests are needed to fully understand the receptivity in flight conditions.

REFERENCES

Agarwal, N.K., Maddalon, D.V., Mangalam, S.M., & Collier, F.S. 1992 Crossflow vortex and transition measurements by use of multi-element hotfilms. *AIAA J.* **30**(9):2212-2218.

Bellhouse, B.J. & Schultz, D.L. 1966 Determination of mean and dynamic skin friction, separation and transition in low-speed flow with a thin-film heated element. *J.Fluid Mech.,* **24**:379 – 400.

Bippes, H. 1991 Experiments on transition in three-dimensional accelerated boundary layer flows. In *Proc. of the Royal Aero. Soc. Conf. on Boundary-Layer Transition and Control*.

Bippes, H. & Müller, B. 1990 Disturbance growth in an unstable three-dimensional boundary layer. In *Numerical and Physical Aspects of Aerodynamic Flows*, Vol. 4, (ed. T. Cebeci), pp. 345-358, Springer-Verlag.

Carpenter, A.L., Saric, W.S. & Reed, H.L. 2009 In-flight receptivity experiments on a 30-degree swept-wing using micron-sized discrete roughness elements. *AIAA Paper* 2009-590.

Haynes, T.S., & Reed, H.L. 2000 Simulation of swept-wing vortices using nonlinear parabolized stability equations. *J. Fluid Mech.* **29:**245-283.

Kosinov, A.D., Semionov, N.V. & Yermolaev, Y.G. 2009 Experiments on the wave train excitation and wave interaction in spanwise modulated supersonic boundary layer. In *Proc. of Seventh IUTAM Symposium on Laminar-Turbulent Transition*, pp. 513-516, Springer.

Mangalam, S.M., Maddalon, D.V., Saric, W.S., & Agarwal, N.K. 1990 Measurement of crossflow vortices, attachment-line flow, and transition using microthin hotfilms. *AIAA Paper* 90-1636.

Pfenninger, W. 1977 Laminar flow control - Laminarization. AGARD Rep. No. 654 (Special course on drag reduction), Von Karman Inst., Rhode-St.-Genese, Belgium.

Press, W.H. 1992 *Numerical Recipes in C: The Art of Scientific Computing*, pp. 575-579 Cambridge UP.

Radeztsky, R.H. Jr., Reibert, M.S. & Saric, W.S. 1999 Effect of isolated micron-sized roughness on transition in swept-wing flows. *AIAA J.* **37**, 1371-1377.

Radeztsky, R.H., Reibert, M.S. & Takagi, S. 1993 A software solution to temperature-induced hotwire voltage drift. In *Proc. of the Third International Symposium on Thermal Anemometry.*

Reibert, M.S., Saric, W.S., Carrillo, R.B. Jr., & Chapman, K.L. 1996 Experiments in nonlinear saturation of stationary crossflow vortices in a swept-wing boundary layer. *AIAA Paper* 96-0184.

Rhodes, R.G., Carpenter, A.L., Reed, H.L. & Saric, W.S. 2008 CFD analysis of flight-test configuration for LFC on swept wings. *AIAA Paper* 2008-7336.

Saric, W.S. 1994 Görtler vortices. *Annu. Rev. Fluid Mech.* **26**, 379-409.

Saric, W.S. & Reed H.L. 2003 Crossflow instabilities – Theory & technology. *AIAA Paper* 2003-771.

VITA

Name: Matthew Jeffery Woodruff

Address: Texas A&M University, Department of Aerospace Engineering
                      H.R. Bright Building, Rm. 701, TAMU 3141
                      College Station, TX 77843-3141

Email Address: woodrufm1@gmail.com

Education: B.S., Mechanical Engineering, Milwaukee School of Engineering,
                      2008

                      M.S., Aerospace Engineering, Texas A&M University, 2011